Defense Threat Reduction Agency
8725 John J. Kingman Road, MS
6201 Fort Belvoir, VA 22060-6201

DTRA-TR-18-6

TECHNICAL REPORT

Fundamental Aspects of Single Molecule and Zeptomole Electroanalysis

April 2018

HDTRA1-11-1-0005

Richard Crooks et al.

Prepared by:
The University of Texas at Austin
105 E 24th St.
Stop A5300
Austin, TX 78712

DESTRUCTION NOTICE:

Destroy this report when it is no longer needed.
Do not return to sender.

PLEASE NOTIFY THE DEFENSE THREAT REDUCTION AGENCY, ATTN: DTRIAC/ RD-NTF, 8725 JOHN J. KINGMAN ROAD, MS-6201, FT BELVOIR, VA 22060-6201, IF YOUR ADDRESS IS INCORRECT, IF YOU WISH IT DELETED FROM THE DISTRIBUTION LIST, OR IF THE ADDRESSEE IS NO LONGER EMPLOYED BY YOUR ORGANIZATION.

REPORT DOCUMENTATION PAGE

Form Approved
OMB No. 0704-0188

1. REPORT DATE *(DD-MM-YYYY)*	**2. REPORT TYPE**	**3. DATES COVERED** *(From - To)*
00-04-2018	Technical	August 8, 2011 - June 1, 2017

4. TITLE AND SUBTITLE

Fundamental Aspects of Single Molecule and Zeptomole Electroanalysis

5a. CONTRACT NUMBER

5b. GRANT NUMBER
HDTRA1-11-1-0005

5c. PROGRAM ELEMENT NUMBER

6. AUTHOR(S)

Richard M. Crooks (PI) The University of Texas at Austin
Allen J. Bard (Co-PI) The University of Texas at Austin
Keith J. Stevenson (Co-PI) The University of Texas at Austin
Bo Zhang (Co-PI) University of Washington

5d. PROJECT NUMBER

5e. TASK NUMBER

5f. WORK UNIT NUMBER

7. PERFORMING ORGANIZATION NAME(S) AND ADDRESS(ES)

The University of Texas at Austin
105 E 24th St
Stop A5300
Austin, TX 78712-1224

8. PERFORMING ORGANIZATION REPORT NUMBER

9. SPONSORING / MONITORING AGENCY NAME(S) AND ADDRESS(ES)

Defense Threat Reduction Agency
8725 John J. Kingman Road, STOP 6201
Fort Belvoir, VA 22060-6201

10. SPONSOR/MONITOR'S ACRONYM(S)

DTRA

11. SPONSOR/MONITOR'S REPORT NUMBER(S)

DTRA-TR-18-6

12. DISTRIBUTION / AVAILABILITY STATEMENT

Distribution Statement A. Approved for public release, distribution is unlimited.

13. SUPPLEMENTARY NOTES

14. ABSTRACT

The objective of this research program was to provide the fundamental understanding required for using the principles of electroanalytical chemistry to detect target molecules at very low concentration, including single molecules, with high specificity, simplicity, and low power. Attainment of this objective required fundamental investigations of reaction kinetics, catalytic activity, nanoparticle synthesis, adsorption, and signal enhancement at surfaces. The results of this study lay the groundwork for detecting and responding to the presence of low levels of CB agents.

15. SUBJECT TERMS

eaction kinetics, catalytic activity, nanoparticle synthesis, adsorption, signal enhancement at surfaces

16. SECURITY CLASSIFICATION OF:			**17. LIMITATION OF ABSTRACT**	**18. NUMBER OF PAGES**	**19a. NAME OF RESPONSIBLE PERSON**
a. REPORT	**b. ABSTRACT**	**c. THIS PAGE**	SAR	44	Anthony Espsoito
Unclassified	Unclassified	Unclassified			**19b. TELEPHONE NUMBER** *(include area code)* 703-767-6046

UNIT CONVERSION TABLE

U.S. customary units to and from international units of measurement*

U.S. Customary Units	Multiply by → / ← Divide by†		International Units
Length/Area/Volume			
inch (in)	2.54	$\times 10^{-2}$	meter (m)
foot (ft)	3.048	$\times 10^{-1}$	meter (m)
yard (yd)	9.144	$\times 10^{-1}$	meter (m)
mile (mi, international)	1.609 344	$\times 10^{3}$	meter (m)
mile (nmi, nautical, U.S.)	1.852	$\times 10^{3}$	meter (m)
barn (b)	1	$\times 10^{-28}$	square meter (m^2)
gallon (gal, U.S. liquid)	3.785 412	$\times 10^{-3}$	cubic meter (m^3)
cubic foot (ft^3)	2.831 685	$\times 10^{-2}$	cubic meter (m^3)
Mass/Density			
pound (lb)	4.535 924	$\times 10^{-1}$	kilogram (kg)
unified atomic mass unit (amu)	1.660 539	$\times 10^{-27}$	kilogram (kg)
pound-mass per cubic foot (lb ft^{-3})	1.601 846	$\times 10^{1}$	kilogram per cubic meter (kg m^{-3})
pound-force (lbf avoirdupois)	4.448 222		newton (N)
Energy/Work/Power			
electron volt (eV)	1.602 177	$\times 10^{-19}$	joule (J)
erg	1	$\times 10^{-7}$	joule (J)
kiloton (kt) (TNT equivalent)	4.184	$\times 10^{12}$	joule (J)
British thermal unit (Btu) (thermochemical)	1.054 350	$\times 10^{3}$	joule (J)
foot-pound-force (ft lbf)	1.355 818		joule (J)
calorie (cal) (thermochemical)	4.184		joule (J)
Pressure			
atmosphere (atm)	1.013 250	$\times 10^{5}$	pascal (Pa)
pound force per square inch (psi)	6.984 757	$\times 10^{3}$	pascal (Pa)
Temperature			
degree Fahrenheit (^oF)	$[T(^oF) - 32]/1.8$		degree Celsius (^oC)
degree Fahrenheit (^oF)	$[T(^oF) + 459.67]/1.8$		kelvin (K)
Radiation			
curie (Ci) [activity of radionuclides]	3.7	$\times 10^{10}$	per second (s^{-1}) [becquerel (Bq)]
roentgen (R) [air exposure]	2.579 760	$\times 10^{-4}$	coulomb per kilogram (C kg^{-1})
rad [absorbed dose]	1	$\times 10^{-2}$	joule per kilogram (J kg^{-1}) [gray (Gy)]
rem [equivalent and effective dose]	1	$\times 10^{-2}$	joule per kilogram (J kg^{-1}) [sievert (Sv)]

*Specific details regarding the implementation of SI units may be viewed at http://www.bipm.org/en/si/.

†Multiply the U.S. customary unit by the factor to get the international unit. Divide the international unit by the factor to get the U.S. customary unit.

Department of Chemistry
The University of Texas at Austin
Austin, TX 78712-1224

Grant/Award #: HDTRA1-11-1-0005
Final Technical Report
For the Period 08/08/2011 - 06/01/2017

Fundamental Aspects of Single Molecule and Zeptomole Electroanalysis

By

PI Name: Richard M. Crooks, The University of Texas at Austin
Co-PI: Allen J. Bard, The University of Texas at Austin
Co-PI: Keith Stevenson, The University of Texas at Austin
Co-PI: Bo Zhang, University of Washington

Introduction

The objective of our research program was to provide the fundamental understanding required for using the principles of electroanalytical chemistry to detect target molecules at very low concentration, including single molecules, with high specificity, simplicity, and low power. Attainment of this objective required fundamental investigations of reaction kinetics, catalytic activity, nanoparticle synthesis, adsorption, and signal enhancement at surfaces: our achievements in this regard are described in this final report. The results of our study lay the groundwork for detecting and responding to the presence of low levels of CB agents. Additionally, our investigations of single electrochemical events have allowed us to uncover phenomena and properties that are not apparent by studying processes involving large numbers of molecules, as is typical in conventional electrochemical experiments in which an ensemble average of the data is treated.

Our approach has been to use a novel electrochemical method to greatly amplify the presence of specific molecules or classes of molecules. The project is based on results demonstrating the detection of individual collisions between catalytic nanoparticles and electrodes, a process we call "electrocatalytic amplification" (ECA). The project also relied on our expertise with the following: (1) synthesis of nanoparticles having well-defined sizes, compositions, and structures that result in tailored catalytic and magnetic functions; (2) functionalization of electrodes and nanoparticles with biological probes such as DNA and proteins; (3) new concepts in microfluidic design for manipulating very small amounts of solution and capturing small numbers of labeled targets; and (4) fabrication of nanoscale electrodes having dimensions that are on the same size scale (~ 3 nm) as the catalytic labels used to signal the presence of individual molecules.

Our approach to the problem is illustrated in Figure 1. Here, a target DNA sequence (shown in green) is detected when it switches on an electrochemical reaction. As discussed later in the report, we have used an approach similar to that shown in Fig. 1 to detect single catalytic particles and demonstrated that amplification factors as high as 10^9 can be achieved. Note that although we have chosen to illustrate DNA detection as a model analyte in Fig. 1, the basic approach is also applicable to proteins and small-molecules.

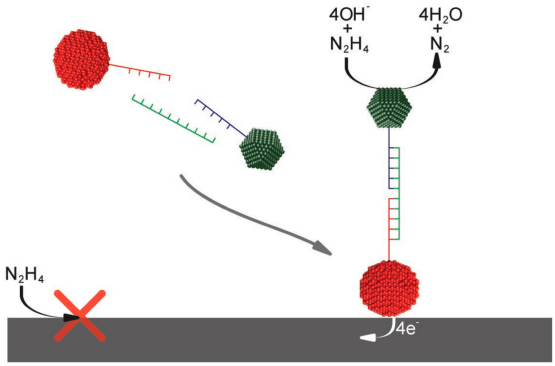

Figure 1. A probe DNA sequence (red) immobilized onto a nanoscale magnetic particle is mixed with a label sequence (blue) modified with an electrocatalyst, such as a Pt nanoparticle. In the presence of the target sequence (green), a sandwich complex forms. Application of a magnetic field in the vicinity of the electrode results in concentration of the complex onto the electrode surface. When an appropriate potential is applied to the electrode an electrocatalytic reaction occurs (here shown as hydrazine oxidation).

Importantly, our team brought together experts in the fields of biosensing, nanoscale electrochemistry, electrochemical theory, nanoparticle synthesis, and fluidic handling with a common goal of enabling detection of low-level chemical and biological agents surrogates.

This was a highly interdisciplinary project, but for the purposes of convenience and accountability this report is organized in terms of research in the individual co-PI laboratories.

Richard M. Crooks – The University of Texas

Summary:
This report details studies conducted by the Crooks group under the support of DTRA grant # HDTRA1-11-1-0005. The main objectives of the Crooks group in this collaboration has been to demonstrate the applicability of single nanoparticle detection via electroanalysis as a sensing platform, with emphasis on the detection of specific oligonucleotides, as well as to optimize reaction conditions to minimize nanoparticle aggregation and increase mass transport to the electrode. The primary system utilized for this purpose was Electrocatalytic Amplification (ECA), which was performed using inert microelectrodes (Au, Hg/Pt, or Hg/Au), hydrazine, and platinum nanoparticles (Pt NPs). In collaboration with the Stevenson group, hybrid platinum/iron oxide nanoparticles were developed, and found to exhibit higher rates of mass transport when subjected to an applied magnetic field. This allowed for much lower limits of detection on the order of attomolar. In addition, aggregation studies of platinum nanoparticles (PtNPs) were conducted and correlated to real-time electrochemical data, allowing for the unambiguous determination of single nanoparticle collisions. Lastly, the Crooks group pioneered the discovery of enzyme-based digestion of platinum nanoparticles (PtNPs), an approach which takes advantage of the fact that conjugating PtNPs with DNA shuts off their electrocatalytic activity. This approach was used to demonstrate successful detection of miRNA targets on Au and Hg/Au microelectrodes.

Introduction:
The goal of this DTRA project is to develop an ultrasensitive single-molecule electrochemistry technique to detect small molecules using the principles of single particle collisions.[1-3] In 2007 the Electrocatalytic Amplification (ECA) technique to electrochemically detect single nanoparticles was developed by the Bard group. This project has focused on gaining a better understanding of this system, applying it to real-world problems, and improving the reaction conditions. In the ECA detection technique, microelectrode composed of an inert material for an inner-sphere reaction in solution is poised a potential where no appreciable catalytic current is passed. Catalytically active nanoparticles are then introduced into the solution, and the collision of these nanoparticles with the electrode surface produces a burst of current corresponding to the redox reaction occurring at the particle surface. These current transients can be analyzed for their amplitude and frequency to gain information about the nanoparticle sample. Although this technique is a powerful tool for detecting nanoparticles, there are three main challenges which the Crooks group has addressed: the limitation of depending on diffusion-based mass transport of these particles to the electrode, the problem of hydrazine-induced particle aggregation, and the challenge of creating a sensor out of this platform.

In detecting very low concentrations of nanoparticles (sub-attomolar), the approach detailed above, which relies on diffusional transport of the particles to the surface of the electrode, is inefficient. The major drawback inherent to the system is that the working electrode must be on the micro- scale in order to detect events with a sufficiently high signal-to-noise and maintain a low background noise. The reliance on diffusion-based transport to a microscale electrode sets a limit of detection for nanoparticles in the range of 10e-14 to 10e-11.[4] To address this limitation and achieve lower limits of detection, the Crooks group conducted a variety of studies on magnetically-driven mass transport of particles, beginning with detection of insulating magnetic beads in microfluidic devices.[5] These studies allowed for the detection of microbeads down to a concentration of 500 zM. Following this study, the Stevenson group published a novel

synthesis for hybrid Pt core, iron oxide nanoparticles.[6] These nanoparticles exhibited both superparamagnetism and electrocatalytic activity for hydrazine oxidation, allowing for increased mass transport via application of a magnetic field, as well as ECA detection. In a joint collaboration between the Crooks group and the Stevenson group, these nanoparticles were tested on both Au microelectrodes, an Au microband in a microfluidic device, and an Au microband in a microfluidic device in the presence of a strong magnetic field.[4] When the magnetic field was applied, it was found that the hybrid nanoparticles exhibited a 6-fold increase in the relative frequency when compared to non-magnetic particles.

A second challenge in the use of an inner-sphere indicator reaction such as hydrazine is the rapid destabilization of platinum nanoparticles in the presence of high ionic strength solutions as well as hydrazine itself.[7] This causes aggregation of the nanoparticles, which leads to decreased frequency of detectable events, as well as variable signals from random aggregates. To address this problem, careful studies correlating colloidal behavior in solution was measured via Nanoparticle Tracking Analysis with ECA data were conducted.[8] Nanoparticle Tracking Analysis is a technique that uses the light scattering from nanoparticles to create individual tracks and calculate diffusion coefficients from their Brownian motion. The time-based aggregation studies, coupled with ECA experiments conducted at different buffer concentrations, confirmed that Pt nanoparticle aggregation is directly related to the ionic strength of the buffer and the presence of hydrazine. The ideal conditions to run ECA experiments in phosphate buffer were concluded to be 5 mM phosphate buffer and 10 mM hydrazine.

In adapting the ECA technology to the detection of small molecules, the Crooks group developed a microfluidic sensor to detect individual DNA hybridization events.[9] In the device, a Au microband was modified with a monolayer of probe DNA. Pt nanoparticles modified with the complementary strand were introduced into the channel, and current transients corresponding to discrete binding events were observed. The sensor was able to detect DNA-DNA binding events down to a concentration of 50 fM target DNA. At the flow rate that these experiments were recorded (50 nL/min), no current transients were observed when Pt nanoparticle-DNA conjugates flowed through the channel in the absence of probe DNA on the electrode surface. Additionally, the sensor was specific, and able to differentiate between the fully complementary target and a partially complementary target DNA.

Further ECA studies revealed, however, that modification of the nanoparticle surfaces with monolayers of DNA affected the magnitude and frequency of ECA collisions.[10] The Crooks group found that although no effects on frequency or size of unmodified Pt nanoparticles were observed when electrode surfaces of Au and Hg were modified with single-stranded DNA (ssDNA), modifying the nanoparticles did have a significant effect on the ECA traces. When collision experiments using Pt nanoparticles modified with ssDNA were performed on unmodified Au and Hg electrodes, the decrease in collision signal was proportional both to the coverage of the DNA (where higher coverage lead to less signal) and the length of the strand (where a 25 base ssDNA strand had a more profound passivating effect when compared to a 5 base strand).

This proved to be a major challenge to address, and taking advantage of the "signal off" nature of Pt nanoparticle-DNA conjugates led the Crooks group to take an enzymatic digestion-based approach to ECA sensing.[11] By using Exonuclease I, a restriction enzyme that cleaves ssDNA at a free hydroxyl group at the 3' end, ECA current can be recovered from previously passivated Pt nanoparticle-DNA conjugates. On both Au and Hg microelectrode surfaces, about 50% of the original ECA current could be recovered. This provided a basic and general approach

to specific biosensing using ECA, and using this technique, the Crooks group demonstrated the specific detection of microRNA-203,[12] a microRNA that is upregulated in psoriasis and differentially expressed in some forms of cancer. The detection limit was 100 pM, and the sensor showed excellent specificity for the target miRNA versus a single-nucleotide mismatch.

Methods, Assumptions, and Procedures:

Synthesis of 4 nm seed and 25 nm Pt nanoparticles

Pt nanoparticles were prepared according to a previously reported procedure.[13] 4 nm seed particles were synthesized by adding 7.76 mL of a 0.2% solution of chloroplatinic acid to 100 mL of gently boiling water. After one minute, 2.37 mL of a solution containing sodium citrate (1%) and citric acid (0.05%) were added, and the solution was boiled for 30 seconds. Next, 1.18 mL of a solution of 0.08% sodium borohydride, 1% sodium citrate, and 0.05% citric acid were added, and the solution was boiled for 10 minutes. 4 nm seed particles were obtained after cooling to room temperature.

To obtain larger nanoparticles on the order of 20-25 nm, 1.0 mL of the Pt nanoparticle seed solution was added to 29.0 mL of water at room temperature. While stirring, 0.023 mL of a 0.4 M chloroplatinic acid solution and 0.5 mL of a solution containing 1% sodium citrate and 1.25% L-ascorbic acid was added. The solution was then heated to boiling at a rate of 10^{o}C/minute. The total reaction time was 30 minutes, and the solution was then cooled to room temperature to yield 20-25 nm Pt nanoparticles. Both Pt seed and larger Pt nanoparticles were dialyzed in a 35 mm dialysis sack (12,000 Da MWCO) and submerged in 4 L of water for 24 hours to remove excess salts. The nanoparticles were characterized using transmission electron microscopy, scanning electron microscopy, and Nanoparticle Tracking Analysis.

Synthesis of Hybrid Iron Oxide/Pt nanoparticles

Iron oxide/Pt nanoparticles (Pt-IONPs) were synthesized according to a procedure outlined by the Wang group, with modifications.[14] 5 nm Pt seeds were prepared according to the procedure outlined above. For the synthesis of Iron oxide/Pt dimer particles, 20 mL of 1-octadecene and 1 mL of oleic acid were mixed and degassed using nitrogen gas, then elevated to a temperature of 120 degrees Celsius. 0.14 mL of iron pentacarbonyl were added. The mixture was reacted for 10 minutes, after which 1 mL of oleylamine was added followed by 20 mg of the Pt nanoparticle seeds (in a 2 mL hexane dispersion, 10 mg/mL). The solution was heated to 300 degrees Celsius and kept at this temperature before cooling to room temperature. The resulting product was purified by precipitating in ethanol and isolated by centrifugation. The particles were washed with 3 cycles of dispersing in hexane, precipitating in ethanol, and centrifugation. The particles were characterized using scanning emission electron microscopy (STEM), energy dispersive X-ray spectroscopy (EDX), X-ray diffraction (XRD), thermogravimetric analysis (TGA), flame atomic absorption (FAA), and X-ray photoelectron spectroscopy (XPS).

Fabrication of Au Microfluidic devices

The microfluidic channel (3 mm x 27 micrometers x 19 micrometers) for the devices was fabricated using standard micromolding techniques and cast in poly(dimethylsiloxane).[15] 4 mm inlet and outlet reservoirs were punched through the PDMS using a hole punch. The base of the device consisted of a glass slide, onto which an Au microband (variable size, depending on the study) had been microfabricated. The PDMS channel and glass slide were then bound together after plasma cleaning.

For magnetism studies, the microelectrochemical cell was attached to a plastic magnet holder, or positioned on top of the focusing magnet.

Electrochemistry

Electrochemical data was obtained using a Chem-Clamp voltammeter-amperometer and a PAR 175 Universal Function generator. The potentiostat and the function generator were connected to a Dell Optiplex 380 computer through a PCI-6251 data acquisition board using a BNC-2090C analog breakout accessory. Electrochemical data was recorded using a custom LabView program, and all experiments were obtained using a custom Faraday cage constructed from copper plate and mesh.

Au, Hg/Pt, and Hg/Au microelectrode preparation

Au microelectrodes (Au UMEs) were polished by wet sanding for 1 minute, then submerged in piranha solution for 1 minute (1:3 30% hydrogen peroxide/sulfuric acid ***Caution!*** *Piranha solution can react violently with organic compounds and should be handled with care.*) Next, they were electrochemically cleaned by immersing in 0.1 M sulfuric acid and cycling the potential between -0.35 V and 1.35 V vs Ag/AgCl for 25 cycles at 0.3 V/s. The UMEs were then rinsed with water and dried under a gentle stream of nitrogen gas.

Hg deposition on platinum microelectrodes was prepared by electrodepositing Hg onto a platinum surface using a previously reported method to form Hg/Pt UMEs.[16] The Pt electrodes were polished via wet sanding for 1 minute. Mercury was then electrodeposited from a solution of 5.7 mM mercury (I) nitrate, 0.5% concentrated nitric acid, and 1 M potassium nitrate at -0.1 V vs Ag/AgCl for 300 seconds. The Hg/Pt UME was then rinsed with water and used immediately.

Hg/Au amalgam microelectrodes (Hg/Au UMEs) were prepared by electrodepositing Hg onto an Au UME according to a previously reported protocol.[17] Following the electrochemical cleaning procedure outlined above for Au UMEs, the Au UME was immersed in a solution of 0.1 M mercury (II) nitrate acidified to pH 1.5 with nitric acid. Mercury was then deposited by applying 0 V vs SCE for 3 minutes, and the UME was removed from solution under potential control, rinsed with water, and used immediately.

Preparation of Pt nanoparticle-DNA conjugates

Pt Nanoparticle-DNA conjugates (PtNP@ssDNA) were prepared using a modified version of a previously reported rapid, pH-assisted conjugation method.[18,19] 400 microliters of the PtNP stock solution were mixed with 5 microliters of 10 or 100 micromolar ssDNA (10 micromolar for the Exo I studies, and 100 micromolar for DSN studies) and incubated at room temperature for 5 minutes. Next, 25 microliters of 100 mM citrate-HCl buffer pH 3 were injected and mixed into the solution, and the solution rested for an additional 5 minutes. 5 microliters of the citrate-HCl buffer were then added, and the solution incubated at room temperature for 25 minutes. Next, 400 microliters of HEPES buffer pH 7.4 were added, and the solution was centrifuged at 16.6 g for 20 minutes, washed with water, and resuspended in Taq buffer (75 mM Tris-HCl, pH 8.8, 2 mM magnesium chloride, 0.01% Tween 20, and 20 mM ammonium sulfate).

Enzymatic assay (Exonuclease I and Duplex Specific Nuclease) Procedures

For the Exonuclease I (Exo I) studies, 30 U of Exo I were combined with 400 microliters of PtNP@ssDNA solution in Taq buffer. The temperature was then elevated to 37°C for 1 hour with gentle mixing at 200 rpm.

For the Duplex Specific Nuclease (DSN) studies, varying concentrations of miRNA solution were added to 400 microliters of PtNP@ssDNA conjugate solution in Taq buffer. After a 20 minute incubation at 25°C, 4 U of DSN were added to the solution, and the temperature was elevated to 42°C for 4 hours with gentle mixing at 200 rpm. After the reaction was completed, the particles were washed three times with water and resuspended in water before immediate use.

Results and Discussion:

Pre-concentration of Particles via Magnetic Enrichment

This DTRA grant has given the Crooks group resources to increase the rate of mass transport of particles to an electrode surface via magnetism. The proof-of-concept was achieved using insulating beads in a microfluidic device. The configuration of the device is shown in Figure 1a, and the device was positioned on top of a sliding magnetic holder. The flow rate and flow direction was controlled using differential heights of solution at each reservoir, as shown in Figure 1b. The mechanism of electrochemically detecting the beads was not ECA, but an electrode blocking mechanism first shown by Lemay and co-workers.[2] The solution in the microchannel contained 5.0 mM ferrocenedimethanol and 50 mM pH 7.0 phosphate buffer. This relatively high buffer concentration was used to minimize the effects of electromigration on mass transport, as the beads had a net negative surface charge. In Case I in Figure 1c, ferrocenedimethanol is oxidized at the electrode surface, and a constant anodic current is observed. In Case IIa and Case IIb, which demonstrates the typical electrode blocking experiments in the absence of a magnet, the insulating bead comes in sufficiently close proximity (Case IIa) or in physical contact (Case IIb) with the electrode, blocking redox current from that particular site on the electrode. This is observed as a sharp decrease in current, and allows for the detection of individual insulating beads. In Case III, the Crooks group demonstrated significantly higher frequencies of collision events when a magnetic field was applied to the electrode. These results are shown in Figure 2. A significant increase in the frequency of current transients due to insulating bead collisions was observed after applying the magnetic field, and a limit of detection of 500 zM.

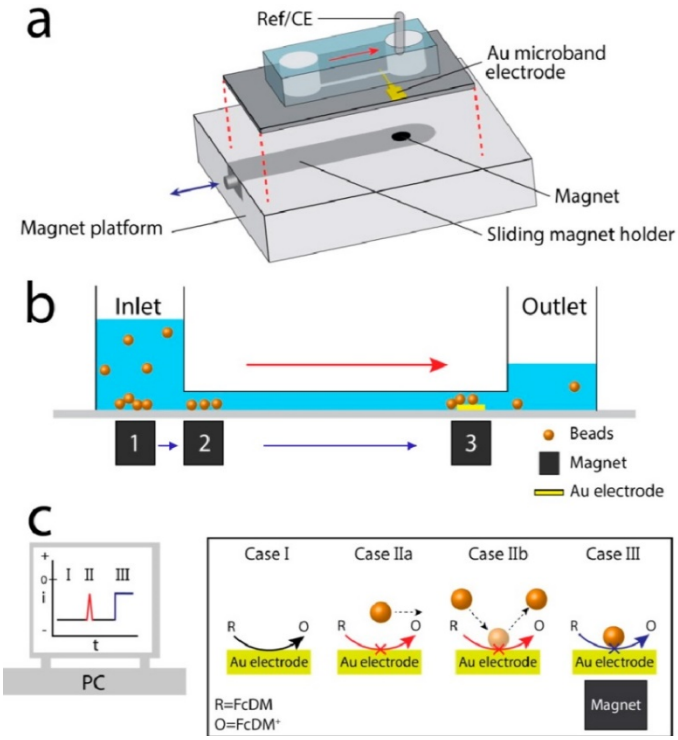

Figure 1. (a) Schematic showing the experimental setup for detecting insulating magnetic beads in a microfluidic device. **(b)** The flow is pressure-driven, controlled by differential fluid heights at each reservoir **(c)** Schematic outlining the possible cases of electrode-solution-bead interactions during the electrochemical experiments.

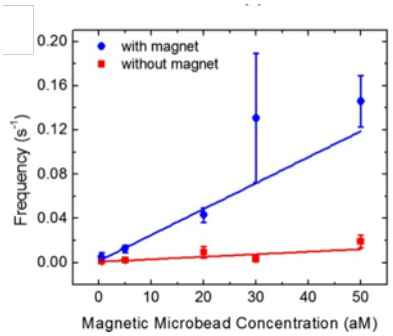

Figure 2. Plot of the frequency of current transients as a function of microbead concentration in the absence (red) and presence (blue) of a magnetic field.

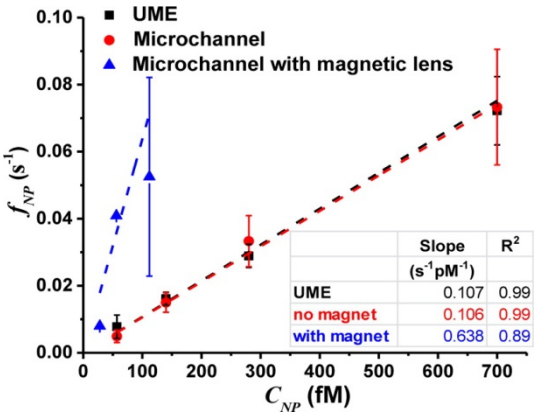

Figure 3. Summary of Pt-IONP collision frequency analysis. Results are shown for Au UMEs (black), Au microband with no magnet applied (red), and Au microband with magnetic lens (blue).

This principle was then applied to increase mass transport of ECA particles: specifically, hybrid iron oxide/Pt nanoparticles (Pt-IONP) synthesized by the Stevenson group.[4,6] These novel nanoparticles were found to exhibit bifunctionality: that is, they exhibited both catalytic activity for hydrazine oxidation (and thus, were capable of ECA detection) as well as magnetic properties for magnetic enrichment. The results for these studies are shown in Figure 3. These experiments were performed with 15 mM hydrazine in solution.

The Crooks group conducted studies within microfluidic devices, with and without application of a magnetic lens, and the frequency of the collision events as a function of Pt-IONP concentration was plotted. When a magnetic field is applied to the electrode surface, a 6-fold increase in frequency of events was observed, thus demonstrating that magnetic enrichment was a viable technique to increase the rate of mass transport and reach low limits of detection.

Pt nanoparticle aggregation studies

A second challenge that needed to be addressed when considering ECA as a sensing platform was the problem of colloidal instability when citrate-capped Pt nanoparticles are suspended in hydrazine/phosphate buffers of net ionic strength greater than 70 mM. To better understand this phenomenon and make more informed decisions regarding solution conditions, careful aggregation studies were conducted by a collaboration of the Stevenson and Crooks groups.[8] To achieve this, real-time aggregation over the span of a typical ECA experiment was monitored with a technique known as Nanoparticle Tracking Analysis, which provides size and concentration information about a colloid solution based on the particles' light scattering properties. The results for solutions of PtNPs suspended in various concentrations of phosphate buffer and 10 mM hydrazine are shown in Figure 4. It was found that increasing ionic strength lead to increased aggregation rates, and larger average hydrodynamic diameters. Additionally, this finding was directly correlated to the ECA behavior of electrochemical experiments conducted in these buffer concentrations on Hg/Pt UMEs. Example traces are shown in Figure 5. The general trend showed that increased phosphate buffer concentrations led to less frequent collision signals with less uniform sizes, indicative of PtNP agglomerates.

Oligonucleotide Sensing with ECA

The Crooks group also developed a sensor that detected individual DNA hybridization events in a microfluidic device using the principle of ECA for real-time detection.[9] This experiment was carried out in a device configured with an Au microband as the working electrode, and the surface of this electrode was modified with ssDNA probe strands. They chose a flow rate of 50 nL/min to flow in 4 nm PtNPs modified with the complementary strand, and at this particular flow rate, current transients due to hydrazine oxidation were observed when strands on the PtNP and those on the electrode would hybridize. Importantly, at this same flow rate, no current transients were observed when only PtNP@ssDNA were injected into the microchannel. No current transients were observed when a PtNPs modified with a non-complementary strand were flowed into the channel with a probe-modified electrode, indicating that the sensor is specific. The limit of detection is also remarkably low: The Crooks group was able to detect down to 50 fM of target.

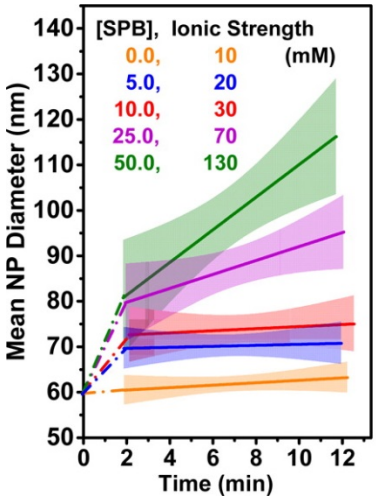

Figure 4. Fitted linear trends of mean hydrodynamic diameter of Pt colloids as determined by NTA. The colored transparent regions are 95% confidence intervals for regression analysis.

Fundamental studies of how modifying nanoparticle and electrode surfaces with DNA affected ECA collisions were also conducted.[10] These studies were performed on both Au and Hg/Pt UMEs, and both a 5-base strand of ssDNA and a 25-base strand of ssDNA were tested. They found that when electrode surfaces were modified with a monolayer of ssDNA, no significant change occurred to the collisions of ECA PtNP collisions when compared to an unmodified electrode for either length of ssDNA. There was no significant difference in the frequencies of these events or the collision sizes for either electrode material. Modification of the PtNP surfaces with ssDNA, however, yielded a significant decrease to both the frequency of events and the size. These results are summarized in Figure 6 for Au UMEs, and a similar trend was observed for Hg/Pt UMEs. Figure 6a shows chronoamperometry data for PtNPs modified with 5 base strand ssDNA. The ratios correspond to the solution modification ratio of ssDNA per PtNP. As the ratio of ssDNA to PtNP increases, the overall current decreases, collision sizes decrease, and collision events become more difficult to resolve. The extent of the decrease in average collision size is shown in Figure 6b. The collision sizes decrease at lower surface concentrations for longer (25-mer ssDNA) versus shorter strands. This finding presented a challenge to the development of an ECA-based sensor. Being able to modify the surface of PtNPs with a high density of DNA is desirable, as this increases the probably of binding events at an electrode surface or in solution.

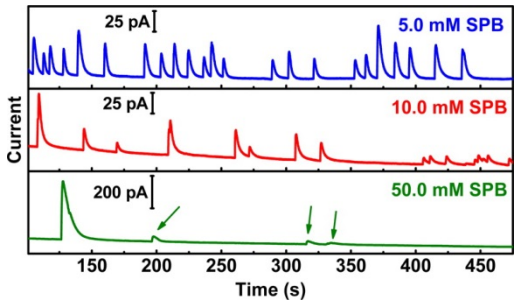

Figure 5. Chronoamperometric traces of current responses for PtNP collisions on Hg/Pt UMEs in three different phosphate buffer concentrations with 230 fM PtNPs.

This problem was addressed with the development of an enzymatic digestion-based proof-of-concept experiment.[11] The general scheme is shown in Figure 7. 20-25 nm PtNPs were

modified at a high concentration of DNA with the same 25-base ssDNA as the previous DNA studies, and this effectively shut off detection of ECA collisions on both Au and Hg/Pt UMEs (Figure 7a). After exposure of these PtNP@ssDNA conjugates to Exonuclease I, an exonuclease specific for cleavage of ssDNA that initiates cleavage at a free –OH on the 3' end of DNA, at least some of the DNA is digested from the surface. Exposing these digested PtNP@ssDNA to hydrazine solutions in ECA conditions shows reactivation of collision signals, as shown in Figure 7b. The Crooks group found that about half of the original collision current could be recovered using this technique on both Au and Hg/Pt UMEs.

Following this development, the Crooks group has developed a sensor based on this concept for the specific detection of microRNA (miRNA).[12] Detection of miRNAs are of biological importance, as different strands of miRNAs have been found to be differentially expressed in certain kinds of cancer. The detection scheme for this sensor is presented in Figure 8. As before, Figure 8a shows that PtNPs are modified with a high surface concentration of ssDNA complementary to the target miRNA. The concentration of miRNA of interest is then introduced into the PtNP@ssDNA solution (Figure 8b) and allowed to incubate at room temperature. Incubation with DSN at 42°C allows for specific cleavage of the ssDNA portions of DNA/RNA duplexes (Figure 8c), leaving the miRNA intact and free to bind with other ssDNAs (Figure 8d). The nanoparticles are then washed, resuspended in water, and tested in hydrazine for

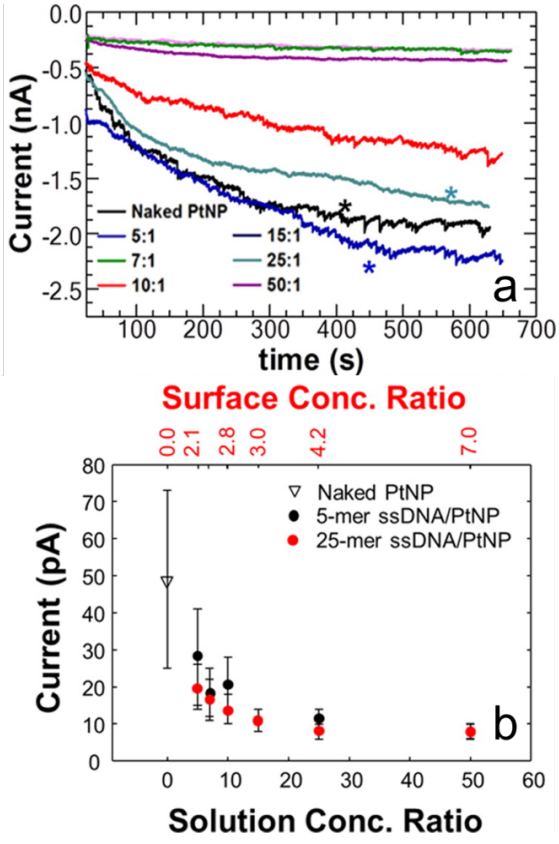

Figure 6. (a) Chronoamperometry data for PtNP@ssDNA modified with 5-mer ssDNA. (b) Plot showing the decrease in collision sizes with increasing coverage of both 5-mer (black) and 25-mer ssDNA.

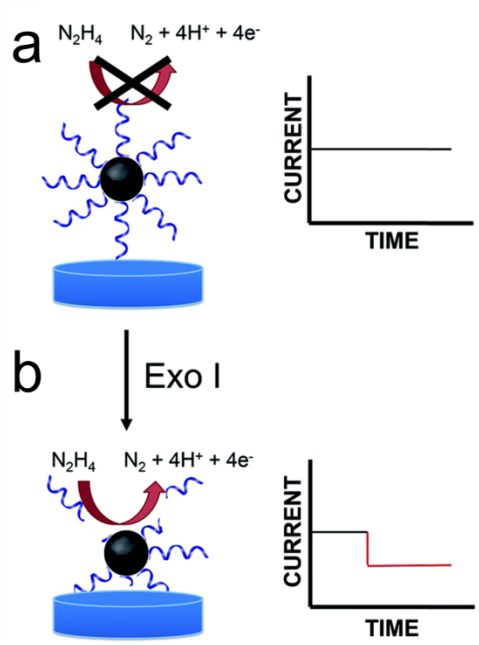

Figure 7. Scheme demonstrating the concept behind enzymatic digestion of PtNP@ssDNA to recover ECA collisions. (a) Deactivation of collisions via high surface concentration of ssDNA (b) Reactivation following Exo I digestion.

collision activity (Figure 8e). The Crooks group found that there was a linear correlation for concentration of miRNA-203, a miRNA upregulated in human psoriasis, at concentrations ranging from 100 pM – 10 nM when analyzing the frequency of 10 pM of the DSN-digested nanoparticles.

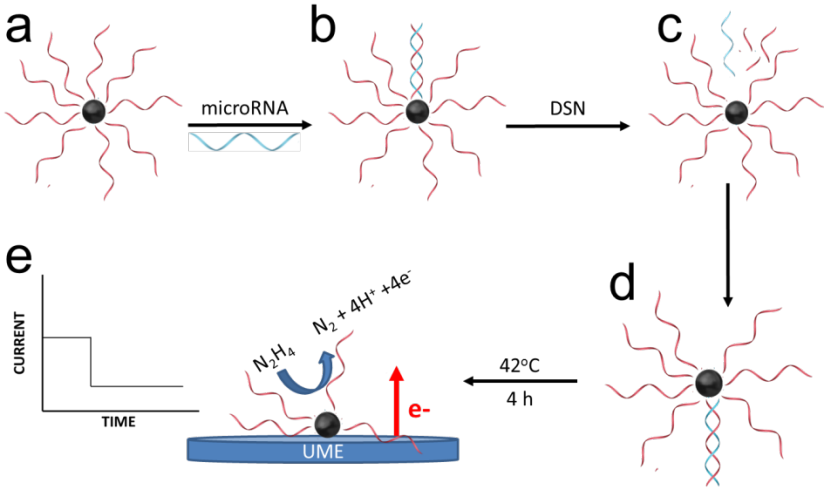

Figure 8. Scheme illustrating the detection method for miRNA quantification using ECA collisions and DSN-based digestion

Conclusions:

This DTRA grant has allowed the Crooks group to solve major challenges that needed to be addressed with single nanoparticle collision electrochemistry, specifically, that of mass transport of particles to the electrode surface, and addressing the issue of particle aggregation in working solutions. Importantly, it also supported the efforts in the development of a sensor using the ECA platform. Detection of oligonucleotides was a major goal outlined in the original proposal for this grant, and the Crooks group demonstrated a viable and specific sensor for microRNA. Recent work in the Crooks group has been focused on demonstrating that this approach is applicable and can be easily modified for detection of any general microRNA, as well as finding ways to improve the detection limit.

Keith J. Stevenson – The University of Texas/Skolkovo Institute of Science and Technology

Summary

This report summarizes studies conducted by the Stevenson group under the support of DTRA grant # HDTRA1-11-1-0005. The main objectives of the Stevenson group in this collaboration has been to demonstrate the applicability of single nanoparticle detection via Electrochemical Amplification (ECA) as a sensing platform, with emphasis on the synthesis of catalytic nanoparticles as electrochemically active labels, as well as to optimize the reaction conditions to

minimize nanoparticle aggregation and optimize the detection of single nanoparticle collisions, which was performed using inert microelectrodes (Au, Hg/Pt, Bi/Pt), indicator probe reactions (hydrazine oxidation, proton reduction) and a library of newly synthesized nanoparticle labels. In collaboration with the Crooks group, Pt- nanoparticles of various sizes, shapes and morphologies were synthesized as well as unique hybrid nanoparticles including Pt/Fe_3O_4 and heterodimer Pt/Au. The most important finding was the use of Hg-based electrodes and hybrid catalytic nanoparticle tags with optimized buffer concentrations allowed for much higher analytical sensitivity (enhanced S/N), wider dynamic range and lower limits of detection (attomolar). In addition, ECA was demonstrated as a new means to follow the kinetics of Pt nanoparticle aggregation and correlated to real-time electrochemical detection of single nanoparticle collisions, allowing for the unambiguous determination of single entity events.

Introduction

The objective of this collaborative project was to provide the fundamental understanding required for using the principles of electrocatalytic amplification (ECA) to detect target molecules at very low concentration, including single entities such as molecules and nanoparticles with high specificity, simplicity, and throughput. We sought investigations of single electrochemical events that have allowed us to uncover phenomena and properties that are not apparent when monitors processes involving ensemble methods involving a large number of molecules, as in conventional electrochemical experiments such as voltammetry and chronoamperometry. Almost a decade ago, Bard and coworkers pioneered the ECA strategy[1] for detecting single nanoparticle (NP) electrocatalysts in solutions containing reactive molecules such as hydrazine, O_2, and protons and as detection probes. In amperometric ECA studies, an ultramicroelectrode (UME) is employed, where the UME substrate is electrochemically inert to the ECA probe molecules at the applied potential. A sharp burst in current is observed when the catalytic NP contacts the UME due to the resulting electrocatalytic oxidation (e.g. hydrazine) or reduction (e.g. protons) of the reactive species in solution. The characteristic shape of the ECA impact signal depends on the composition and physical properties of the electrode material.

Of the various ECA detection strategies developed over the course of the past nine years, the most commonly employed scheme involves citrate-stabilized Pt NPs as the catalysts and hydrazine as the reactant species. To date, the majority of ECA have used very simple ~5- nm to 50 nm Pt nanoparticles as labels. To fully understand and optimize the ECA process, the Stevenson group considered alternative sizes, shapes, and compositions to separately optimize both the magnetic capture and catalytic the amplification factors required for zeptomole and sub-zeptomole detection. Magnetic and catalytic nanoparticles were prepared by a new synthetic method to make hybrid Pt-decorated iron oxide NPs (Pt-IONPs) consisting of a magnetic core and a catalytic shell. This synthesis yields stable colloidal suspensions of crystalline nanoparticles having an average particle size (~) and shape that can be controlled by adjusting reaction conditions (e.g., temperature and precursor concentration). As detailed by collaborations with Crooks these hybrid Pt-IONPs exhibited both superparamagnetism and electrocatalytic activity for hydrazine oxidation, allowing for increased mass transport via application of a magnetic field, as well as ECA detection. They were tested on both Au microelectrodes, an Au microband in a microfluidic device, and an Au microband in a microfluidic device in the presence of a strong magnetic field.[4] When the magnetic field was applied, it was found that the hybrid nanoparticles exhibited a 6-fold increase in the relative frequency when compared to non-magnetic particles.

Another major challenge that emerged over the course of this work was evidence of Pt NP aggregation while conducting ECA experiments with hydrazine and phosphate buffer at pH 8 using 3-5 nm Pt NPs and Au UMEs.[7] Specifically, Koper et al. showed that the Pt NPs were distributed as large branched aggregates on Au and pointed out large distributions of the measured current step ECA events which increase in polydispersity with increasing hydrazine concentration. Koper attributed the aggregation to specific interactions of hydrazine at the citrate/Pt interface and noted that the fractal dimension of the aggregates appeared to fit the growth model of diffusion-limited aggregation (DLA). Our own groups have characterized hybrid Pt-IONPs) using nanoparticle tracking analysis (NTA)[4,6,20] and showed that the as-synthesized Pt-IONPs were suspended as aggregates in deionized water and maintained their average hydrodynamic size after exposure to 15 mM N_2H_4 and 50 mM phosphate buffer. Similarly, we found that the resulting rate of Pt-IONP impacts (impact frequency as a function of particle concentration) with a Au disk UME agreed well with theoretical predictions of diffusion-limited transport based on particle sizing and quantification by NTA, in contrast to previous reports of citrate-capped Pt NPs in comparable ECA solution conditions.[1,21] Since experimentally determined ECA impact rates involving citrate-stabilized Pt NPs and N_2H_4 have been found to be much slower than predicted,[1,21] we then commenced studies using time-resolved NTA to monitor changes in NP size and concentration, which made it possible to systematically interrogate the rapid diffusion-limited aggregation kinetics of Pt NPs under different solution conditions. Direct comparison of data from the NTA and ECA experiments provided fundamental insight into how colloidal interactions affect the analysis of NP/electrode impacts. This information served to guide optimization of experimental conditions necessary for stabilizing a monodispersed Pt NP label and ultimately allowed for the confident interpretation of ECA event signals as truly representing single, not aggregated, NP impact events. Impact rates were then found to agree with prediction based solely on diffusion, as confirmed by constructing a calibration curve of impact frequency to NP concentration and comparing the ECA-derived diffusion coefficient with the estimation based on SEM sizing and the Stokes-Einstein-Sutherland relations.

Methods, assumptions, and procedures

Synthesis of citrate capped Pt nanoparticles

Citrate stabilized Pt NPs of various sizes ere synthesized according to procedures described in Crooks section of this final report.

Synthesis of Hybrid Iron Oxide/Pt nanoparticles

Iron oxide/Pt nanoparticles (Pt-IONPs) were synthesized according to a procedure outlined in Crooks section of this final report.

Nanoparticle Tracking Analysis

Nanoparticle tracking analysis (NTA) was performed using the ns500 instrument from Nanosight, Ltd. The NTA method of optical single-NP detection is based on dark-field scattering microscopy; light source is a blue 488 nm laser. The transport of each optically detected NP that diffuses through the detection volume is recorded by a camera. In post-acquisition processing the diffusive trajectories are analyzed by tracking algorithms to estimate size based on their Brownian motion assuming spherical NP geometry. NTA simultaneously provides an estimate of the NP concentration throughout the acquisition time by directly counting the total number of

NPs in the fixed detection volume and averaging the sum of NP counts per acquired camera frame. The final results of NTA provide the overall NP size distribution acquired from a single video recording. These distributions were analyzed it different time increments and calibrated to the estimated mixing time. The Pt NP stock suspension was treated in an ultrasonic bath for 30 minutes prior to a new NTA experiment to fully reconstitute Pt NPs, which slowly concentrate to the bottom of over the course of a few days for the case of citrate-capped 50 nm Pt NPs in water. This settling behavior was confirmed to be reversible by sonication because NTA of the Pt NP standards in water reproducibly resulted in a mean diameter of 64(±8) nm. Each NTA sample was prepared by diluting a 20 μL aliquot of purified Pt NP stock suspension to 4 mL with the chosen hydrazine/buffer system and immediately transferred (within 5 s) to the NTA instrument inlet tube for fluidic sample loading. The time of sample loading was used to calibrate the sample mixing time. NTA measurements could only be acquired after ~100 s of NP mixing because of the combination of NTA fluidics loading time and a delay period for allowing fluidic convection to subside. All NTA size distributions were compiled using more than 1000 individual Pt NP tracking measurements. The NTA-measured size distribution represents the measurement with the least amount of individual NP tracks in this work, 1100±800 tracked and analyzed Pt NPs for the three replicate acquisitions. Zeta potential measurements were performed at an applied electrokinetic driving voltage of 24 V for samples in water, 8 V for 25 mM Tris sulfate and 10 mM sodium phosphate buffers, and 12 V for all other samples.

Electron Microscopy

Scanning transmission electron microscopy (STEM) was performed using a Hitachi-S5500 microscope operated at 30 kV equipped with a Bruker Quantax 4010 EDX detector. Samples were prepared for electron microscopy by dropping nanoparticle suspensions onto Formvar-coated TEM grids and drying at 60°C over the course of 3 days to fully evaporate water. Scanning electron microscopy (SEM) was performed using a Hitachi-S5500 microscope operated at 5 kV. Samples were prepared by lowering a piece of stainless steel foil into two different ECA solutions (10 mM N_2H_4 and 5 mM SPB, pH 7.8 and 10 mM N_2H_4 and 50 mM SPB, pH 7.8) for two hours and allowing them to adsorb the Pt NP aggregates.

Electrochemical Instrumentation and Hg/Pt Ultramicroelectrode Fabrication

All electrochemical experiments were performed with a two-electrode setup controlled by an electrochemical workstation (CH Instruments, Austin, TX, model 700). Prior to acquiring a series of NP impact measurements, Hg was electrodeposited on a 10 μm diameter Pt UME disk. Briefly, a step potential of -0.5 V versus mercury-mercury sulfate reference electrode (CH instruments) was applied for 333 s to a home-made Pt UME immersed in 5.7 mM mercury nitrate in 0.5% HNO_3 in 1 M KNO_3. The resulting spherical cap Hg UME was rinsed gently with water before immersing in the hydrazine test solution for nanoparticle impact measurements. The same individual Pt UME disk was reused as the deposition substrate by reproducibly depositing and stripping the Hg droplet before and after a day's worth of ECA experiments.

ECA aggregation studies

Prior to performing ECA experiments on a new buffer system, the saturated calomel reference electrode (SCE) was immersed into a small compartment cell filled with 1.5 mL volume of the test solution. The reference cell was constructed from a glass tube with a high porosity glass frit sealed at its base. The entire reference cell assembly was lowered into a small

vial containing 4 mL of the test solution until the glass frit base was fully submerged. The complete electrochemical cell was housed in a Faraday cage and purged with Ar before a NP impact experiment. A CA trace was recorded at the applied potential of 0 V vs. SCE for about 100 s to establish a smooth flat current vs. time baseline before injecting a 20, 15, 8, or 4 μL aliquot of the stock NP solution for a final concentration of 1.1, 0.85, 0.45, and 0.23 pM, respectively. An aliquot of the stock Pt NP suspension was agitated in a sonication bath for at least 30 min prior to an injection. Quickly after injection the solution was gently bubbled with Ar for ~5 s to ensure proper distribution of Pt NPs in solution and then switched to Ar blanket over the cell. CA events for NP impact frequency analysis were sampled from a 400 s time interval after 15 s post-injection delay time to allow bubbling-induced hydrodynamic convection to subside. The stability of the Hg superhemispherical droplet was evaluated by optical microscopy before and after a full series of experiments at the studied Pt NP concentration, and confirmed to maintain its geometric dimensions within 10-20% relative error. Only ECA impact signals with a current magnitude of 3 times the standard deviation of the peak-to-peak noise or higher were included in the NP impact frequency analysis. For the colloidally stable 5 and 10 mM SPB samples, the ECA-derived diffusion coefficients were compared to those estimated by SEM sizing and the Stokes-Einstein-Sutherland relation: $D_{NP}=(k_B T)/(3\pi\eta d_{NP})$

Here DNP is the Pt NP diffusion coefficient, kB is the Boltzman constant (1.38×10-23 J/K), T is temperature (298 K), η is the solution viscosity (0.89 mPa·s), and dNP is the mean NP diameter measured with SEM.

The NP frequency was calculated by applying a custom moving sum-average with Excel spreadsheet. Specifically, the frequency for the first ten impacts was calculated by dividing the sum total by the elapsed time after Pt NP introduction. All other events after the 10th impact were counted as a total of 10 events divided by the time in between the first event of the set and first event of the next ten impacts. This data processing was also applied in the backward direction starting at the end time and the two forward/backward results were averaged together. The scatter data was fit to the Smoluchowski coagulation equation as a custom function in Origin 2016 data analysis package.

Results and discussion

Pre-concentration of Particles via Magnetic Enrichment

The process of magnetic enrichment to increase mass transport of ECA particles using newly synthesized hybrid iron oxide/Pt nanoparticles (Pt-IONP) from the Stevenson group was examined in detail in collaboration with the Crooks group. As detailed in Crooks section of the final report these novel nanoparticles were found to exhibit both catalytic activity for hydrazine oxidation (and thus, were capable of ECA detection) as well as magnetic properties for magnetic enrichment. The studies are summarized by Crooks and will not be detailed here.

Pt nanoparticle aggregation studies

As described in Crooks section of this report our groups conducted a series of experiments to understand the problem of colloidal instability when citrate-capped Pt nanoparticles are suspended in hydrazine/phosphate buffers of net ionic strength greater than 70 mM. These studies are summarized by Crooks and will not be reported here. Yet we note that the electrochemical NP impact method is sensitive to changes in the bulk particle concentration and size distribution, which establishes ECA as another viable method for reporting on NP aggregation kinetics. As shown in Crooks section representative CA traces of ECA collision

events for three different buffer conditions were conducted. The CA traces present the same relative trend of decreased ECA signal frequency in higher ionic strengths. Much larger ECA signals in terms of both current magnitude and Hg deactivation time are observed for the 50 mM SPB sample, indicating the electrode impacts of large NP aggregates. At higher Pt NP concentrations, a more pronounced aggregation effect is observed for the 50 mM SPB sample, displaying very large/broad NIE signals that complicate the analysis of smaller impacts. At the lowest ionic strength, the impact signal frequency and amplitude remain relatively consistent throughout the recorded time period, indicating that Pt NP size does not change very much over the time scale of the analysis because conditions are favorable for colloidal stability.

The ECA signal frequencies were analyzed at varied Pt NP concentrations (Figure 1) to understand the effect of aggregation on NP transport to the UME/solution interface. The overall NP/UME impact frequency is expected to be directly proportional to both NP concentration and average diffusion coefficient according to diffusion-limited transport to the spherical cap Hg UME:

$$R_{NP} = f_{NP}{C_{NP}}^{-1} = 2\pi\beta N_A D_{NP} a_{UME}$$

Here R_{NP} represents the rate at which NPs collide with the Hg UME, fNP is the frequency of NP impacts at a given NP concentration (C_{NP}), N_A is Avogadro's number, D_{NP} is the NP diffusion coefficient, and a is the basal radius of the Hg spherical cap (5 µm for Pt disk UME substrate). The term β is a size dependent constant for the super-hemispherical cap family of UMEs. The Hg UME was reproducibly grown as super-hemispherical with surface area that is on average 1.84-fold larger than a perfect hemisphere with 5 µm radius, giving a β value of 1.35. According to the equation above, the NP impact frequency is proportional to C_{NP} and D_{NP}, both of which decrease over time for an aggregating Pt NP sample. As shown in Figure 1, the NP impact frequency is inversely proportional to ionic strength, which correlates to the same general trend of NP concentration as monitored by NTA. For a stable dispersed colloid, f_{NP} should increase linearly with NP concentration. Linear calibration curves were established for the two lower ionic strength conditions. The difference in the slope between the 5 and 10 mM SPB samples (blue and red curves) indicates their relative stabilities, with the 5 mM condition being most stable. The limit of detection for the 5 mM SPB condition is 160 fM Pt NP for a 400 s CA acquisition time. The calculated NP diffusion coefficients based on the NIE slope (R_{NP}, Equation above) for the two optimized systems of lower ionic strength correlate well with NTA for Pt NP samples measured under identical solution conditions and in deionized water. Shown for further comparison is the calculated D_{NP} using diameters of individual Pt NPs measured by SEM,

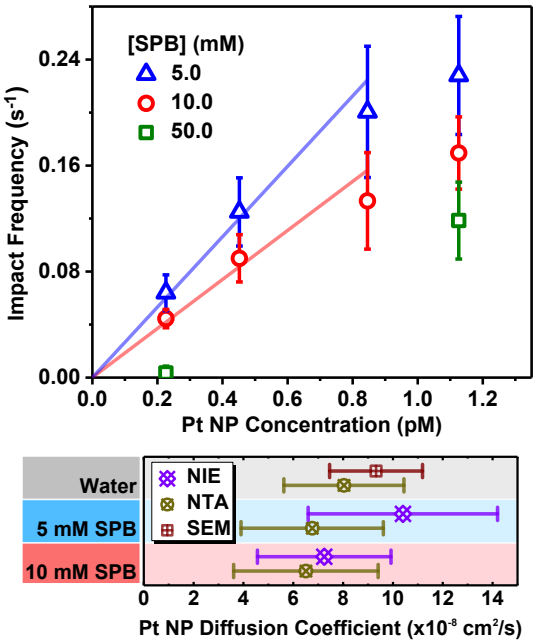

Figure 1. NP impact analysis. Top panel: impact event frequency (event counts per 400 s sampling from 15-415 s post mixing) plotted with respect to NP concentration in the presence of 10 mM N_2H_4 with different SPB concentrations; vertical bars are standard error of 5 replicate ECA(NIE) measurements. Bottom panel: NP diffusion coefficients approximated from SEM, ECA(NIE), and NTA.

which also lies within the range of error for the NIE experiments. The ECA collision rates obtained in previous studies of 3-4 nm Pt NPs by Bard and coworkers were calculated to correspond to an apparent diffusion coefficient of ~1×10^{-8} cm^2/s. This value is one order of magnitude slower than what we obtain here for NPs that are ten times larger in diameter. We suspect that the reason for the previously reported DNP value is likely due to rapid NP aggregation because experiments involved unoptimized solution conditions (e.g. 50 mM phosphate buffer and 15 mM N_2H_4) that do not support citrate-stabilized Pt colloids. The previously proposed kinetic limitations on observed NP impact event frequency for this system should therefore be reconsidered with the inclusion of colloidal instability effects. For the optimized 50 nm Pt colloids, however, the unprecedented agreement of the NIE system with NTA and SEM characterizations confirms that the observed ECA signals resulted from single NP impacts on a Hg UME.

The combined results of the ECA and NTA colloidal characterizations in the optimized experiments confirm that observed electrochemical signals using phosphate-buffered 10 mM N2H4 solutions of < 20 mM ionic strength are predominantly the result of electrocatalytic hydrazine oxidation on individually dispersed 50 nm Pt NPs after colliding with a Hg UME. The establishment of quantitative correlations between ECA and NTA significantly aid in ongoing pursuits to develop ECA for applications such as colloidal NP size characterizations, evaluations of catalytic activities at the single NP level, and strategies for ultrasensitive bioanalysis.

Having established the conditions for detecting single Pt NPs impacts via ECA, we then utilized this methodology to follow aggregation kinetics in real time using ECA correlated with NTA.

Figure 2 shows Pt NP size distributions over time as monitored by NTA for the aggregation inducing 50 mM SPB + 10 mM N_2H_4 condition. Figure 2b, shows the corresponding mean NP diameters plotted over a time of 1 h. After 30 min of aggregate growth, a linear growth region is observed corresponding to an average aggregation rate of 3.8 nm min-1. Figure 2c shows the natural log of the aggregate diameter divided by the initial 50 nm diameter, ln(d/dp), as a function of $\ln(t/\tau)$, where t is time and τ is the time constant for the rate of coagulation, which was determined to be roughly 240 s, which is the time when the NP concentration decreases to have its initial value (Figure 2a). The ln-ln plot in Figure 2c clearly shows two different rate regimes, the earlier one is slow followed by an abrupt transition to a faster rate regime after 30 minutes. The slow growth region indicates reversible coagulation. For the fast rate a fractal dimension (δ) of 1.0 from the inverse slope of the plot in Figure 2c is obtained, indicating a linear structure of the Pt NP aggregates. The inset electron micrograph in Figure 2b shows a small linear chain of four Pt NPs that aggregated naturally during solvent evaporation on the hydrophobic carbon film coated TEM grid. The SEM images in Figures 3 and 4 show the aggregate structures formed in the presence of two ECA buffers that we've investigated previously with NTA and NP impact rate analysis. For these experiments, a piece of stainless steel foil was lowered into the ECA solution and left to adsorb the Pt NP aggregates that formed over the course of 2 hours. Figure 3 shows a mixture of primary 50 nm Pt NPs and small aggregates containing no more than 5 primary NP units that adsorbed on the metal surface in 10 mM N_2H_4 + 5 mM SPB solution. In Figure 4, we see larger aggregates that formed in the higher ionic strength 10 mM N_2H_4 + 50 mM SPB solution, as expected. Chain-like NP aggregates appeared in both figures along with some that adopted more closely packed arrangements.

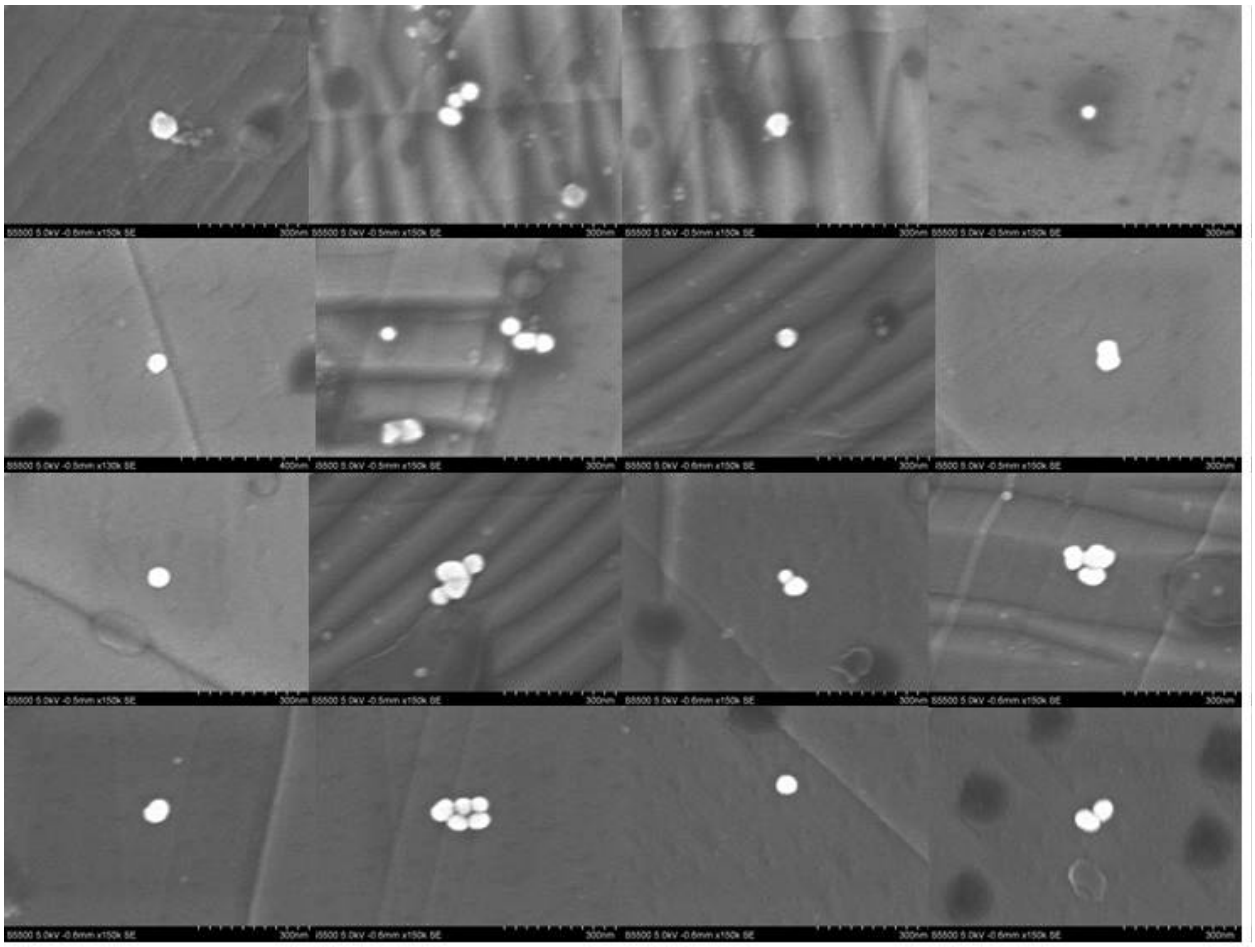

Figure 3. SEMs of Pt NPs adsorbed on stainless steel foil after from solution of 10 mM N_2H_4 + 5 mM SPB, pH 7.8 over the course of one hour at 1.1 pM Pt NP concentration.

We suggest that Pt NPs are directed to assemble in a linear fashion by stronger bridging interactions and large electrostatic repulsive contributions from the densely adsorbed citrate on the surface. However, one must also consider the heterogeneity of the Pt nanograins on the NP surface. Some of these crystallites may be much more active than others for N_2H_4 decomposition. We are not sure exactly how this relates to aggregation. It could create pressure-driven repulsion if the rate of decomposition is sufficiently fast and bubbles are released at a continuous frequency. In this sense, we are proposing that the Pt NPs may be behaving like nanomotors. If the gas is building up from within the Pt NP, then this could eventually rupture the stabilizing citrate layer at a specific site and further promote linear assembly.
An alternate explanation for the nanobubble hypothesis is the hydrazine is becoming a part of the H-bonded citrate network. N_2H_4 could very well function as both H-bond donor and acceptor. The N_2H_4 may be donating H to the carboxyl groups of citrate and create a strong bridging interaction, thus cross-linking the Pt NPs by interparticle H-bonding to induce aggregation.

The combined results of these experiments support that the stability of citrate on Pt involves much more than just electrostatic interactions. A structure based on intermolecular H-bonding in the citrate capping layer appears to be the most likely explanation for the exceptional stability of these large Pt NPs in 50 mM ionic strength with buffer salt in the absence of hydrazine. The stability was evidenced by the range of reversible metastability (agglomeration)

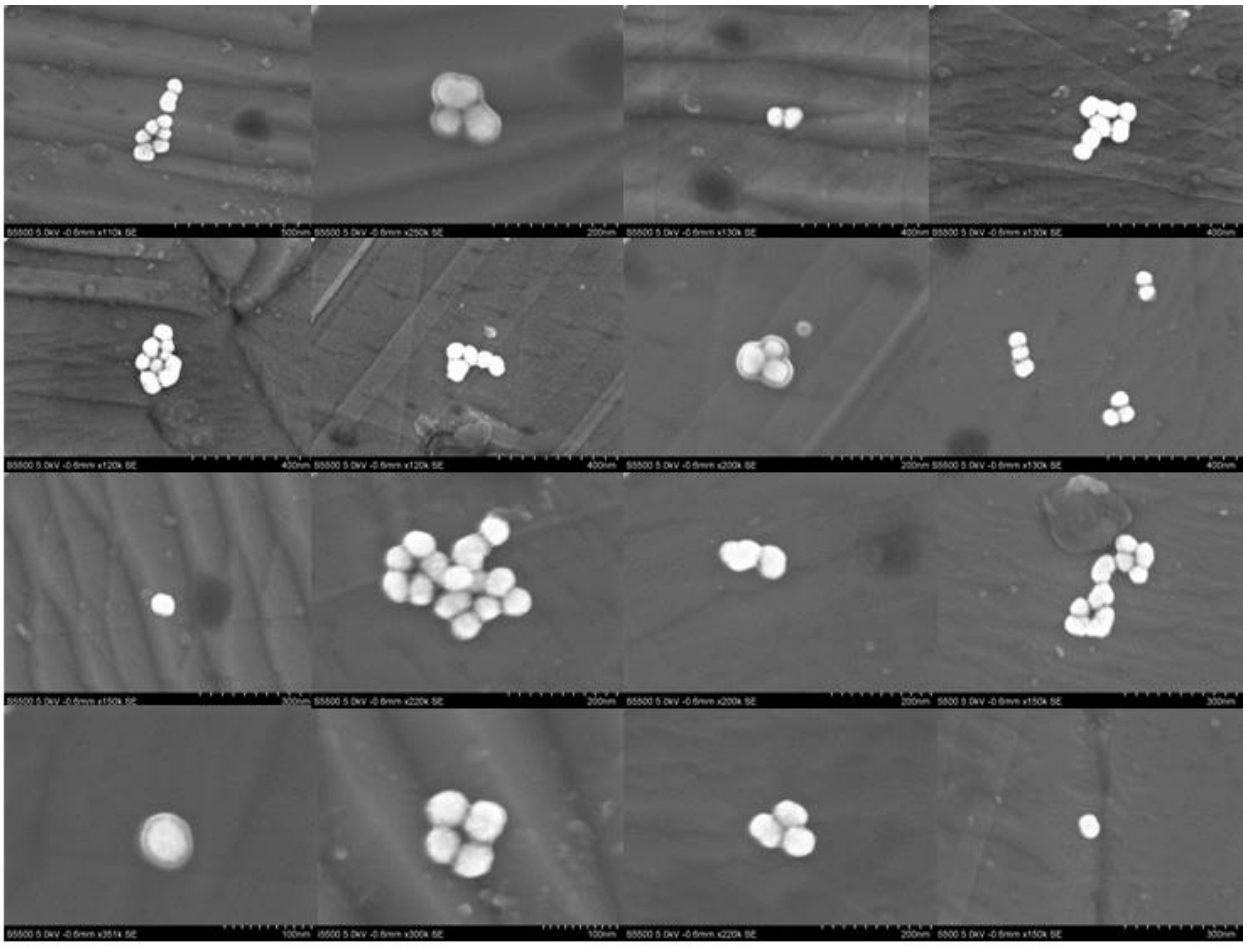

Figure 4. SEMs of Pt NPs that adsorbed on stainless steel foil from solution of 10 mM N_2H_4 + 50 mM SPB, pH 7.8 over the course of one hour at 1.1 pM Pt NP concentration.

before linear directed assembly of Pt NP chains. The mechanism of Pt NP aggregation includes specific reactive contributions from hydrazine; whereas, the hydrazine decomposition is thought to occur to some extent at the citrate-coated Pt surface. According the OCP measurements utilizing a Pt wire, the citrate remains adsorbed on the Pt surface even after treating with 10 mM and 100 mM N_2H_4. This result is most likely true for the Pt NPs as well. Although citrate stays stuck to the Pt and does not undergo substantial ligand-exchange with hydrazine, we expect that the membrane-like structure is disrupted by evolved gaseous decomposition products and ruptures, causing instability and promoting coagulation. The heterogeneity of the nanostructured Pt NP surface is expected to influence the aggregation mechanism and induce polarity by bridging interactions, which we expect to involve both a higher degree of interparticle H-bonding at the terminal primary NPs of the chain in the presence of hydrazine and the physicochemical contributions from Pt-catalyzed hydrazine decomposition products. We demonstrated proof of concept using ECA based as a method for quantifying Pt NPs aggregation kinetics with suitable time resolution to that of other methods such as NTA.[20]

Conclusions

This DTRA grant has allowed us to elucidate several parameters for perfecting ECA based methods for quantitative single NP detection. Several parameters were optimized such as

hydrazine concentration, ionic strength, pH as well as indicator electrodes (Hg/Pt) that enable single nanoparticle collision electrochemistry, specifically, of that addressing the issue of particle aggregation in working solutions. Importantly, Stevenson in collaboration with Crooks group aided in the development of a sensor using the ECA platform for detection of oligonucleotides. The final work also established ECA as a means to study aggregation kinetics of NP at sufficient concentration and time resolution that is competitive with other methods such as nanoparticle tracking analysis (NTA). These efforts enabled the establishment of several analytical figures of limit (detection limits, dynamic range and analytical sensitivity) for quantitative detection and analysis of ECA methods.

Allen J. Bard – The University of Texas

Summary:
Throughout the course of the DTRA project, new advances have been made in the area of ultrasensitive detection of analyte species. To achieve these advances, new techniques and procedures have been developed using advanced electrochemical techniques to specifically detect and quantify analyte species at the sub-picomolar level. Analyte species that have been part of the project include emulsion droplet, platinum nanoparticles, and virus particles.

Introduction:
Electrochemistry is a powerful tool that stands poised to begin studying the chemical and physical properties of single entities. In 2004, Serge Lemay published a landmark paper describing the observation of discrete adsorption events of microspheres onto microelectrodes.[22] Since that time, a variety of other nanoparticles have been studied (*vide infra*). This new field of study has many exciting ramifications. One relatively unexplored area is that if these collisions can be made specific, the limit of detection inherent in these experiments is the ultimate sensitivity in chemical analysis: one (one small molecule, one protein, one virus, one nanoparticle, one cancer cell.) Another ramification is that chemical and physical information can be probed on the single entity level, such as how the size and shape of a nanoparticle impacts that particle's catalysis.

In Lemay's landmark report, the authors described a method that one could use to detect single insulating microspheres on ultramicroelectrodes (UMEs). The experimental details are simple: The oxidation of ferrocene methanol was driven at the surface of the UME by applying a potential step to a potential where the oxidation of ferrocene methanol is mass-transfer limited. When insulating microspheres are introduced to the solution, and a single microsphere is incident on the electrode surface, the oxidation of ferrocene methanol will be blocked, which manifests as a stepwise decrease in current in the amperometric i-t trace. Figure 1 gives a schematic representation of this experiment, which is termed blocking. In panel A, a heterogeneous reaction is driven at the electrode surface. When this reaction is driven, a concentration gradient is set up at the electrode surface, which is shown by the faded blue hemisphere immediately outside the disk electrode surface. An amperometric i-t trace shows a non-zero current consistent with the steady state current to a disk electrode with a certain concentration of R initially in solution. Panel B shows the introduction of insulating beads (orange in color) into solution. If the concentration of ions in solution is high enough (>25 mM), mass transfer of the beads is governed largely by diffusion and not electrophoretic migration. The flux of these microspheres to the electrode surface can be understood in a stochastic sense by considering the frequency with which the microspheres collide with the electrode in the absence of migration or

convection. Panel C shows the amperometric i-t response when a particle randomly diffuses near the electrode and begins perturbing the concentration gradient of reactant. A decrease in current occurs. Panel D shows the response when this bead completely collides with the electrode, and Panel E shows a new steady-state current value is reached.

Unfortunately, it is difficult to extract meaningful information from the magnitude of size of the blocking event in amperometry (i.e., the magnitude of the step-wise decrease in current). Because radial diffusion dominates at the edge of a microelectrode, the current density will be

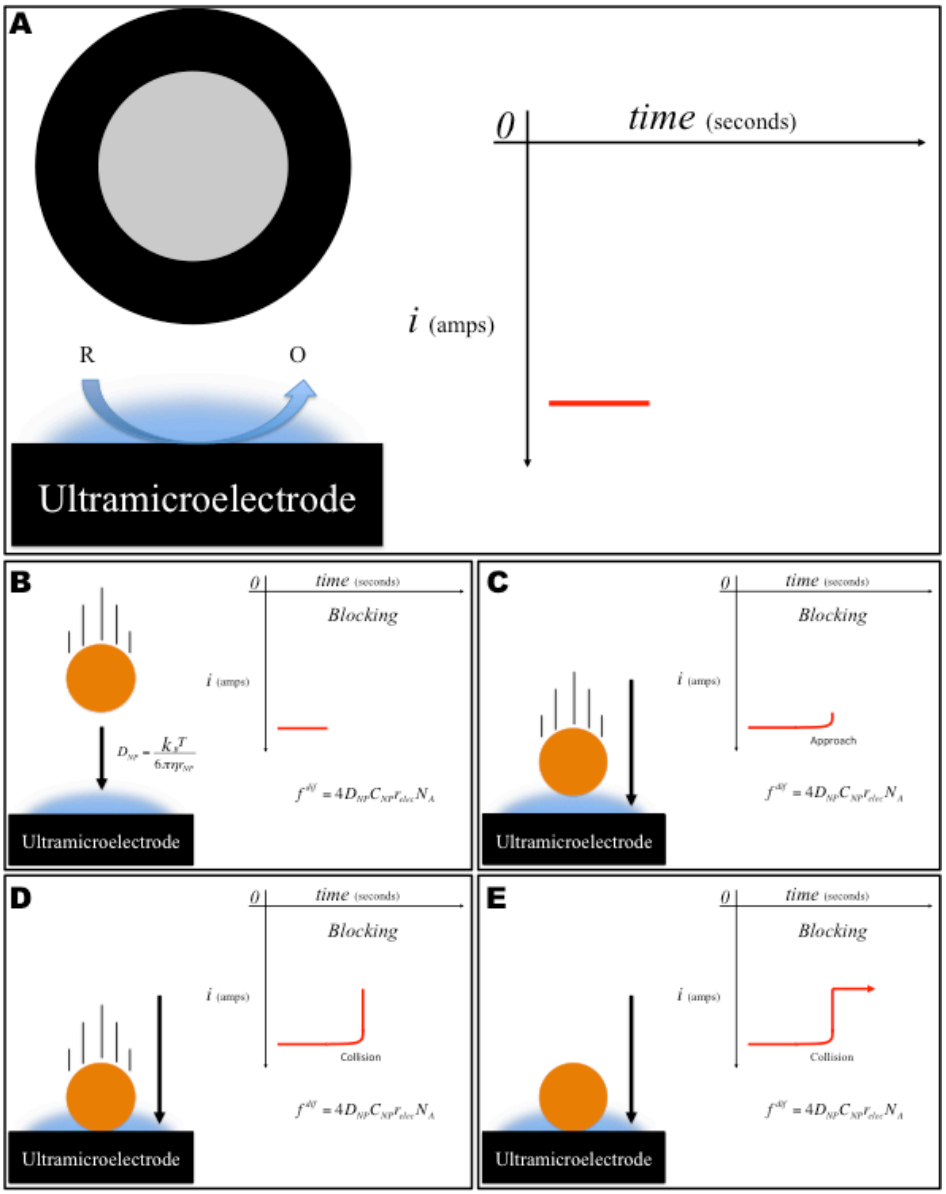

Figure 1: Schematic representation of the blocking experiment. A.) An electrochemical reaction is carried out at the UME surface, and a concentration gradient is formed (faded blue near the UME). The amperometric i-t trace measures the current at an applied potential at the mass transfer limit of the electrochemically active analyte. B.) Insulating nanoparticles (orange circles) are introduced into the system. C.) Particles diffuse by random walk to the electrode surface, which can be seen in the amperometry as a decrease in current. D.) Particles irreversibly adsorb to the electrode surface. E.) Particles stick to the electrode surface, which is observed in amperometry by the step-wise decrease in current followed by a leveling off at a new steady-state current value.

highest at the edges. This implies that a microsphere colliding with the edge of the electrode will block more flux than a microsphere colliding with the center of the electrode. Thus, without visualizing the collisions by correlated microscopy, it is impossible to correlate the colliding species radius to the decrease in current. Furthermore, microspheres colliding with the glass directly around the electrode will also block flux to the electrode surface, further complicating the analysis.

Since Lemay's paper in 2004 concerning the discrete detection of insulating microspheres adsorbing to an ultramicroelectrode (UME), stochastic techniques have been developed for many different types of nanoparticles, such as catalytic nanoparticles,[23] silver and copper particles, vesicles,[24,25,26] emulsion droplets,[27] virus particles,[28,29,30] macromolecules,[31] and even cancer cells.[32] Bard and co-workers developed electrocatalytic amplification (ECA) in 2007. In this experiment, conductive, catalytic nanoparticles can be detected. The most widely used experiment for ECA has been the oxidation of hydrazine, which proceeds quickly on platinum, slowly on gold, and slower yet on carbon. The key in these experiments is that the reaction of interest must have much slower kinetics on the substrate electrode than on the colliding nanoparticle, such as hydrazine oxidation or proton reduction. Proton reduction will be discussed mostly throughout this dissertation. Because of the difference in the kinetics of hydrazine oxidation or proton reduction on these different materials, one can envisage an experiment where a gold electrode is biased at a potential where hydrazine oxidation does not occur on gold but will occur on platinum. When a platinum nanoparticle is incident on the electrode surface, it will catalyze the oxidation of hydrazine. If enough faradaic current is produced from the catalytic reaction, the collision of a nanoparticle onto the electrode surface can be observed. Figure 2 gives a schematic representation of the electrocatalytic amplification experiment. In these experiments, the hope was to develop an electrochemical method that is able to quantify the catalytic activity of single NPs and compare those NPs to explore variations in kinetics.

Figure 2 shows a schematic representation of the experiment. In this case, proton reduction occurs very fast on platinum compared to a carbon substrate UME. Thus, if protons are present and a platinum NP is incident on the carbon surface, the faradaic response can be observed when measuring the current as a function of time. Figure 2 also shows the amperometric response, which increases when the NP collides with the electrode surface. At the time of this dissertation, there were many problems associated with these experiments. For instance, instead of observing constant limiting current values after

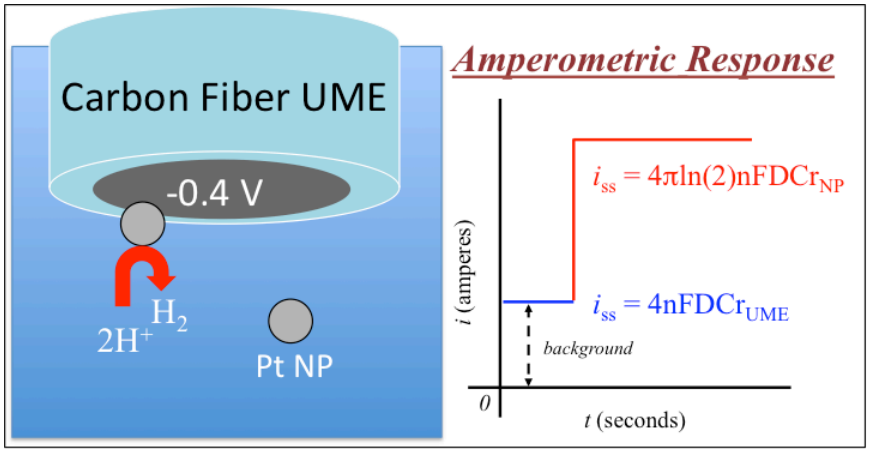

Figure 2: Schematic representation of the electrocatalytic amplification experiment. When a carbon electrode is biased at a potential where proton reduction does not occur on carbon but readily on platinum, a faradaic current will flow when a platinum nanoparticle is incident on the electrode surface, and an increase in steady-state current will be observed.

collision of the NP onto the UME, the current response would often decay over time. This decay has been associated with impurities[33] and bubble formation.[34] White and co-workers, however, have shown that bubble formation should not occur under these general experimental conditions.[35] Also, there are heterogeneities in the synthesis process of making NPs, ambiguous capping agent affects on electron transfer, and NPs tend to aggregate over time and are sensitive to solution species.

Methods, assumptions, and procedures

The experiments were conducted using mainly amperometric and potentiometric analysis techniques, where either the current or potential would be monitored over time. The techniques, some combined with Electrocatalytic Amplification (ECA), could sense minute changes to an electrode such as a collision of a nanoparticle where there was either a decrease in current or as in the case with combined ECA an increase in current or change in measured potential. Typically, very dilute concentrations of nanoparticles (pM - fM) were used in an electrolyte solution with the reactant. These techniques utilized ultramicroelectrodes (UMEs) which were made by sealing a micron sized (12.5 or 25 um Pt or Au) wire into glass and significantly enhance the signal to noise ratio. The electrodes would then be carefully polished prior to use with alumina (0.05 μm) paste on microcloth pads. Monodisperse emulsion systems were created by ultrasonication followed by filtering through a 200 nm porous filter. Discrete droplet collision events were observed in the amperometric i-t curve. Simulations were performed by solving the Poisson and Nernst−Planck equations using COMSOL Multiphysics 3.5a software. The electrostatics and Nernst−Planck without charge neutrality modules were used. An adaptive free triangular mesh element was used. The mesh size at the UME surface was set to 5 nm.

Results and discussion

During the project duration the Bard group has accomplished many significant milestones with many scientific advancements and achievements. The areas that these advancements covers are predominantly in the area of nanoparticles collisions but also include Scanning Electrochemical Microscopy (SECM), fundamental theory for analysis collisions and detection of biologically relevant particles including viruses. Extremely high sensitivities to analyte are achievable using the nanoparticle collision and specifically the electrocatalytic amplification techniques. Concentration as low as femtomolar levels are routinely used but in essence the technique allows for the detection of a single nanoparticle or analyte molecule. More specifics of these advancements are discussed in greater detail below.

The effects of colliding particles that will lead to a change in the electrode area were investigated.[36] In one experiment the electrode area will become blocked and will not be available for a electrochemical reaction to occur, thus effectively shutting off a portion of the electrode and decreasing the electrochemical current. Figure 3A shows how the insulating silica or polystyrene nanoparticles colliding with a Pt UME block the oxidation of reactant. The physical position the particle sticks to the electrode will have an effect on the observed current change. One colliding at the edge of an electrode will decrease the current more than one colliding in the center of the electrode. Figure 3B shows a schematic illustrating how the electrode area can be effectively increased leading to an increase in the rate of a given outersphere reaction signaling the detection of the analyte. One way this is achieved is by the attachment of a large surface area carbon nanotube to a gold nanoparticle.[37] The gold nanoparticle will stick to the platinum electrode allowing the large area carbon nanotube to

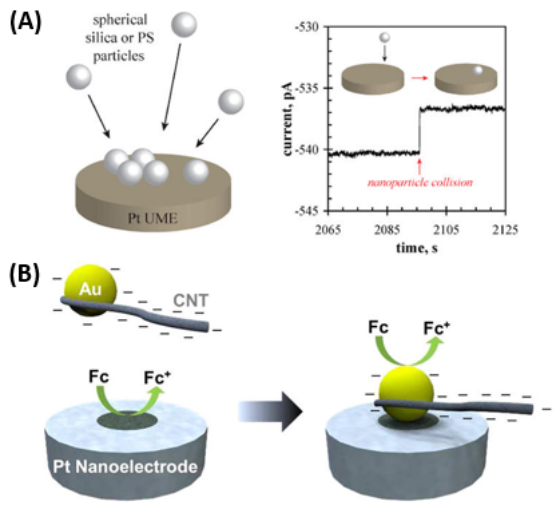

Figure 3: Schematic representations of collisions where the electrode area will be either decreased or increased. (A) Insulating nanoparticles colliding with an electrode surface where the particle block the surface and result in a decrease in the observed current. (B) Gold nanoparticle modified carbon nanotube collision with a nanoelectrode effectively increasing the area of the electrode.

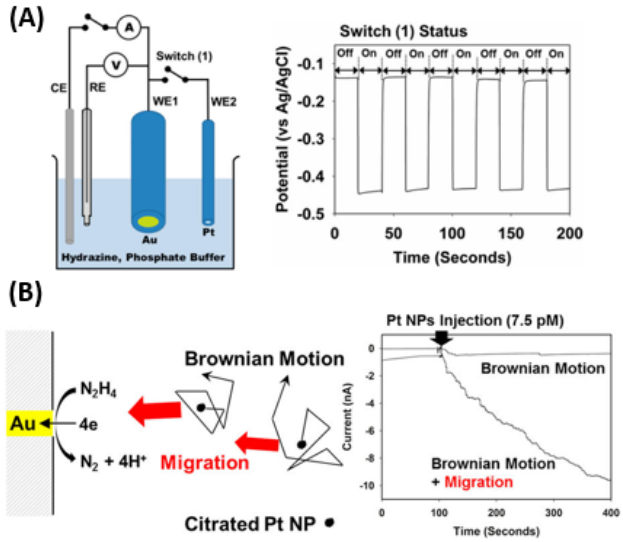

Figure 4: (A) Schematic depicting the effective nanoparticle collision experiments where a Pt nanoelectrode was used as a model nanoparticle and connected by a switch to a Au UME and the magnitude of the OCP change upon switching could be repeatedly measured. (B) Effect of migration on the collision frequency of nanoparticles to a Au UME where the collision frequency is observed to be much higher than predicated for diffusion alone.

facilitate the oxidation of the reactant leading to a significant increase in current. Carbon nanotubes that are not modified with Au nanoparticles will not stick to the electrode and result in a current "blip".

The theory behind nanoparticle collision and resulting observations was also advanced.[38] The change in open circuit potential (OCP) upon particle collision was studied by a mimic experiment looking at the electrode and colliding nanoparticle sizes effect on the magnitude of the change. This was accomplished with Pt nanoelectrodes that were used as model nanoparticles. The nanoelectrode and a larger Au UME were connected by a simple circuit and an electrical switch could be used to connect the electrodes together in solution effectively simulating the nanoparticle collision, shown in Figure 4A. The resulting changes in OCP could be estimated using Butler-Volmer kinetics which could be used to calculate the change at different electrode and nanoparticle size combinations.

The effect of migration on the observed frequency was investigated where the charged NP can also be attracted to the electrode by the electric field in solution causing an enhancement in the collision frequency.[39] The migration of charged NPs is affected by the supporting electrolyte concentration and the faradaic current flow. A simplified model based on the NP transference number is introduced to explain the migrational flux of the NPs. Experimental collision frequencies and the transference number model also agreed with more rigorous simulation results based on the Poisson and Nernst−Planck equations

Additional studies into the theoretical aspect were done to investigate the time of first arrival and how electrophoretic migration of ions and charged nanoparticles (NPs) in low electrolyte concentration solutions affects positive feedback in scanning electrochemical microscopy (SECM).[40] The time of first arrival, which is time from the beginning of the experiment

until the moment of observation of the first nanoparticle collision event, as seen in Figure 5A. This is evaluated as a measure of ultralow (sub-femtomolar) concentration of analytes in solution. Theoretical equations were developed relating the time of the first arrival and the concentration of analyte species in solution for the cases when the species is transferred by diffusion alone and with electrophoretic migration. The use of the multiplexed parallel detection based on simultaneous measurement of a series of time of first arrival values will allow both faster and more precise determination of ultralow concentrations of analytes. The role in an SECM experiment of the strength of the electric field in the gap between either the tip and the substrate, or the tip and counter electrodes, is shown to increase proportionally to the decrease in gap size, shown in Figure 5B.[41] This field affects the flux of the charged redox species as expected for dilute electrolyte solutions. The rate of collisions of charged insulating NPs with the tip electrode decreases as the tip is brought closer to the substrate electrode. This can be explained by the blocking of the particle flux with the glass insulating layer around the metal microwires.

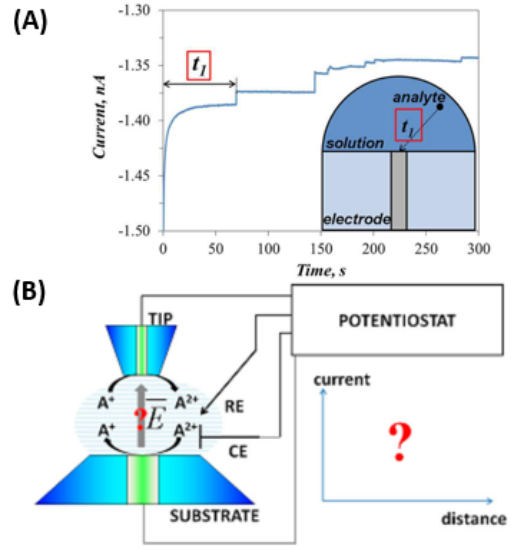

Figure 5: (A) Time of first arrival where the time it takes for the first detectable nanoparticle collision can be an indication of the concentration of particles. (B) Effect of electric field strength on the detection of nanoparticles using SECM.

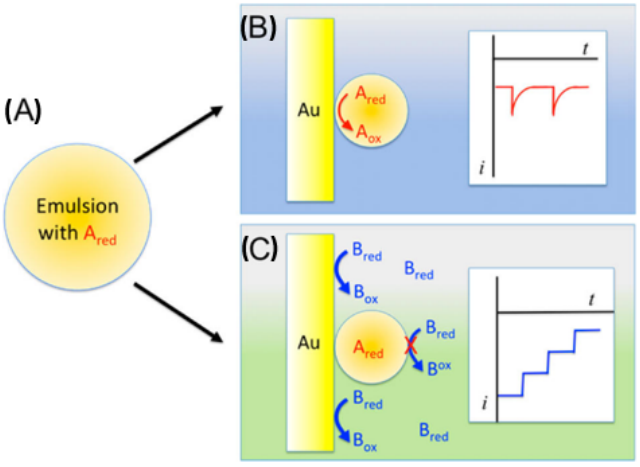

Figure 6: (A) schematic of a emulsion droplet where the interior of the droplet is filled with a liquid that is immiscible with the bulk liquid and can also contain reactant molecules. (B) When a emulsion droplet collides with an electrode surface the reactant present inside the droplet will react resulting in a current spike or blip. (C) Alternatively, an emulsion droplet can block a portion of the electrode preventing reactant in the bulk solution from reacting on the electrode resulting in a decrease in current.

Emulsion droplet collisions were investigated for the first time. These emulsions form nanoscale soft particles and can contain a solution (and reactant molecules) that differ from the bulk solution.[42] These soft particles were investigated in two different methods (Figure 6). In the first method, an electroactive redox species, inside a toluene-in-water emulsion droplet is measured by chronoamperometry during a collision with a (UME) where a blip or spike type of collision signal is observed. The observed current represents the electrolysis of the droplet contents and can be used to determine the size of the droplet. In the second method, electrochemical oxidation of an electroactive redox species in the

continuous aqueous phase is hindered by a droplet blocking collision. In this case, a staircase current decrease is observed. From an analysis of single soft particle collision data, one can find the emulsion droplet size distribution and the droplet contents.

Using the emulsion droplet technique where the droplets contained an electroactive species, discrete collisions of zeptoliter emulsion droplets on a UME can be used as individual controlled potential coulometry experiments.[43] These events of single emulsion droplet coulometry experiments typically only lasted between 100 and 500 ms whereby all the reactant inside the droplet was used up. Each of these collisions are interpreted as individual coulometry experiments, implying that several bulk electrolyses can be carried out over the course of one collision experiment. Knowing the volume of the droplet, Faraday's Law can be employed to calculate the number of electrons per molecule passed during the electrolysis. This new technique can be used to calculate the electron stoichiometry for more complicated systems, such as the oxidation of tetrathiafulvalene (TTF), tertiary aliphatic amines, such as tripropylamine (TPrA), and a 1,2-diphenylhydrazine (DPH) molecule. This electroanalytical methodology allows for fast, nanoscale electrolysis in low dielectric media.

In addition to emulsion droplets different forms of particles incorporating the emulsion functionality were investigated. These were single unilamellar vesicles, composed of a bilayer lipid membrane (BLM) were investigated for the first time, by both the vesicle blocking and vesicle reactor techniques.[44] The vesicle blocking technique can be used for determining the vesicle solution concentration from the collisional frequency and also for observing the vesicle adhesion on the electrode surface. In addition, vesicle reactor (VR) experiments show clear evidence that the lipid bilayer membrane does not collapse or break open at the electrode surface during the vesicle collision. Because the bilayer is too thick for electron tunneling to occur readily, an appropriate concentration of a surfactant was added in the VR solution to induce loosening of the bilayer (transfection conditions). This allowed the electrode to oxidize the contents of the vesicle.

During the course of this project observations of stochastic collisions of murine cytomegalovirus (MCMV) on ultramicroelectrodes (UMEs) were first reported (Figure 7), extending the observation of discrete collision events on UMEs to biologically relevant analytes.[45] This observation was enabled by adsorption of an antibody specific for a virion surface glycoprotein. This allowed differentiation of MCMV from MCMV bound by antibody and selectivity was achieved by interactions between MCMV, a glycoprotein-specific primary antibody to MCMV, and polystyrene bead "anchors," which were functionalized with a secondary antibody. This work extends the field of collisions to biologically relevant antigens and provides a novel foundation upon which qualitative sensor technology might be built for selective detection of viruses and other biologically relevant analytes.

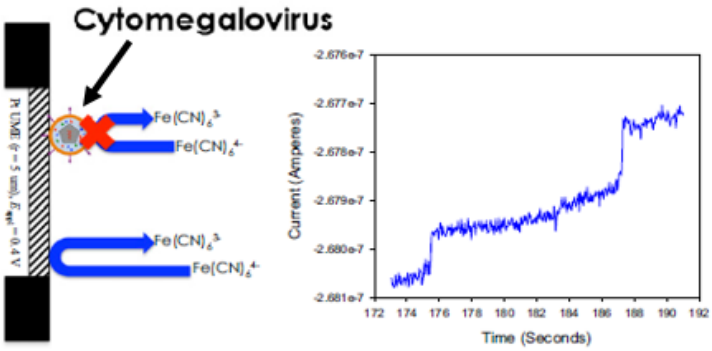

Figure 7: Single virus collision were achieved and studied by the blocking of the electrode resulting in a decrease in observed current.

Conclusions

In conclusion, the field of nanoparticle collisions has been advanced in experimental and theoretical approaches. Understanding the different aspects and effects different conditions has on the detection and analysis of single nanoparticles and molecules will allow the effective limits of detection to become lowered. New methods of analysis have been invented and evaluated for their efficacy and opens up new avenues for electrochemical detection and analysis.

Bo Zhang – University of Washington

Summary

This report describes recent research performed in the Zhang group under the support of this DTRA grant. In this project, research in the Zhang group has been primarily focused on achieving a deeper understanding of nanoparticle collision using several electroanalytical tools including well-characterized nanoelectrodes, fast-scan cyclic voltammetry (FSCV), closed bipolar electrochemistry, and fluorescence-enabled electrochemical microscopy (FEEM). The Zhang group has developed advanced metal nanoelectrodes using both a laser pulling method and microfabrication. These nanoelectrodes have exciting use in both fundamental electrochemistry studies and nanoparticle collision experiments. This project has supported the publication of several invited review articles on the topic of nanoelectrochemistry in several leading analytical chemistry journals including *Analytical Chemistry* and the *Analyst*. The Zhang group has pioneered the use of FSCV to the study of single collision events. The use of FSCV enables one to achieve unique chemical resolution and invaluable kinetic information of heterogeneous electron transfer at single nanoparticle surfaces. Using a higher bandwidth and faster recording speed, the Zhang group has identified interesting ultrashort current spikes associated with nanoparticle collision events when particles are present at higher concentrations in hydrazine solution. A plausible mechanism has been suggested which accounts for the generation of hydrogen molecules from catalytic decomposition of hydrazine molecules on Pt surfaces and the formation of H_2 nanobubbles. The Zhang group has also reported a new method to study collision of Ag and Au nanoparticles on carbon ultramicroelectrodes (UMEs). In order to further address the challenge of low throughput in single molecule sensing experiments, the Zhang group has developed FEEM as a new electrochemical imaging method for simultaneous recording of electrochemical responses from massive electrochemical arrays. FEEM enables one to couple a redox reaction of interest to a fluorogenic redox reaction using bipolar electrochemistry so that the faradaic process can be optically monitored.

Introduction

The overall goal of this DTRA project is the development of an ultrasensitive single-molecule electrochemistry method based on the concept of single-nanoparticle collision.[46,47] The method explored in this work will find use in the detection and quantification of trace amount of clinically relevant biomolecules down to single copies. Research efforts in the Zhang group have been focused primarily on the development and use of structurally well-defined nanoelectrodes and ultramicroelectrodes (UMEs) for mechanistic studies of single-nanoparticle electrochemistry and single-nanoparticle collision. Furthermore, with this support, the Zhang group has accomplished substantially in the areas of fluorescence-enabled electrochemical microscopy

(FEEM)[48] and bipolar electrochemistry[49,50] in general with the goal of extending the collision concept to large-scale electrochemistry arrays for high throughput electrochemical sensing.

The electrocatalytic amplification (ECA)-based detection of single nanoparticle collision is a unique electrochemical approach pioneered by the Bard group[47,51] which has provided the fundamental basis for the proposed research in this DTRA project. In the ECA detection scheme, one detects electrocatalytically active nanoparticles using a more inert UME. In a solution containing a proper inner-sphere redox species, the UME is hold at a potential where there is no detectable redox reaction taking place on the UME itself. Single nanoparticles are detected when they diffuse and make contact with the UME surface catalyzing the redox reaction on their surfaces. In order to more fully utilize the enormous potential of the ECA method for trace detection in a more complex biological environment, it is necessary to develop a more complete understanding of nanoparticle collision using single nanoparticles on a well-controlled nanoelectrode.

Compared to UMEs, nanoelectrodes are electrochemical probes with radii between 1 to 100 nm. Nanoelectrodes offer superior advantages in electrochemical studies such as low noise, high spatial resolution for imaging, and fast kinetic response due to high mass transport rates.[52,53,54] One of the most popular fabrication methods is the use of laser pulling to prepare glass-sealed metal nanoelectrodes.[54] Other useful methods include mass-fabricated metal pyramid nanoelectrodes, nanoelectrode based on the use of carbon nanotubes, carbon-filled nanopipettes, and tunneling nanoelectrodes based on the immobilization of a single nanoparticle on an insulated ultramicroelectrode.[54] The Zhang group has used the laser pulling method to prepare Pt and Au nanoelectrodes down to 1 nm in radii.[55] Besides the above mentioned advantages, nanoelectrodes provide an exciting platform for immobilizing a single nanoparticle during collision experiments so that one can examine and obtain detailed nanoparticle structure information using high-resolution electron microscopy following electrochemical recording.

In the conventional ECA experiments, one records the current change associated with particle collision at a constant holding potential. Despite the high temporal resolution, the amperometric recording has limited chemical information. Recognizing this limitation, the Zhang group has reported the use of fast-scan cyclic voltammetry (FSCV) to record individual collision events on a carbon UME.[56] Their experiments have demonstrated unique chemical resolution and good temporal resolution with FSCV. For example, they reported the detection and recognition of Au and Pt nanoparticles based on simple analysis of their voltammetric responses. Their recent experiments have extended the use of FSCV to the study of heterogeneous electron-transfer (ET) kinetics at single metal nanoparticles.[57]

One of the major challenges in the use of inner sphere redox molecules in the ECA mechanism is the quick destabilization of the analyte nanoparticles in the presence of high concentration redox species. The aggregation of nanoparticles leads to a decreased detection frequency and the observation of more random signals from the aggregated particles. As a result, one usually work with nanoparticles at low concentrations, such as pM. Additionally, the concentration of supporting electrolyte and the buffer conditions have to be carefully controlled. In order to address this challenge, the Zhang group has developed a new indicator reaction for particle collision on carbon UMEs.[58] This new strategy relies on the reduction of AgCl electrochemically deposited on the surface of a carbon UME prior to the collision experiment. Single collision events are detected as small cathodic current spikes when metal nanoparticles catalyze the reduction of AgCl back to Ag.

Many of the previous ECA-based collision experiments have used hydrazine oxidation as the inner sphere redox reaction.[59,60,61] The complete electrochemical oxidation of a hydrazine molecule generates four electrons, one N_2 molecule, and four H^+ and the amperometric signal is often represented as a quick increase in the anodic current followed by a slow decay which is caused by nanoparticle deactivation. It has been previously reported that although hydrazine is stable in water at ambient conditions, it readily decomposes in the presence of a good catalyst to form N_2, H_2, and NH_3 among others.[62] Performing nanoparticle collisions at nM particle concentrations, the Zhang group has observed interesting ultrashort current spikes on top of the conventional staircase current responses.[63] Their experiments have suggested that these ultrashort current spikes are due to electro-oxidation of H_2 nanobubbles generated from hydrazine decomposition.

Conventional nanoparticle collision method has limited throughput when particles are present at extremely low concentration, such as attomolar (aM) or zeptomolar (zM). A low analyte concentration and the use of a small electrode lead to a very low detection frequency. As such, an ultralong recording period may become necessary in order to obtain statistically meaningful results. One attractive method to increase the throughput is the use of a large array of UMEs in which each UME can be separated addressed. However, due to technical limitations in fabrication and recording, it is challenging to record from arrays containing more than 100 electrodes. The Zhang group has been working on the use of coupled electrochemical reactions to record electrochemical responses from massive electrochemical arrays containing >1 million UMEs. The method they developed is called fluorescence-enabled electrochemical microscopy or FEEM. The central idea of FEEM is the use of a bipolar electrochemistry mechanism to couple a redox reaction of interest to a fluorogenic redox reaction so that one can use optical microscopy to monitor electrochemical reactions from numerous electrodes. The use of FEEM has enabled the use of massive electrochemical arrays to image dynamic redox events such as diffusion of dopamine out of a micropipette and electrocatalytic oxidation of H_2O_2. Future use of FEEM will allow simultaneous recordings of nanoparticle collision events on very large UME arrays to substantially increase throughput.

Methods, assumptions, and procedures

Synthesis of 12 nm Au and 4 nm Pt Nanoparticles: Gold nanoparticles were synthesized by the reduction of $HAuCl_4$ with sodium citrate.[64] All glassware was thoroughly cleaned with fresh piranha solution and rinsed thoroughly before use. 50 ml of 0.01% m/v of $HAuCl_4$ was refluxed while stirring and 1.8 ml of sodium citrate solution (1% m/v) was then rapidly injected into the flask. The solution was allowed to reflux for 15 minutes and then allowed to cool to room temperature.

Platinum nanoparticles were synthesized according a previous report.[65] Using thoroughly cleaned glassware, 36 ml of a 0.2% chloroplatinic acid hexahydrate was added to 464 ml of DI water. The solution was brought to a boil and 11 ml of 1% sodium citrate and 0.05% citric acid was added. After a ~30 seconds, 5.5 ml of freshly prepared 0.08% sodium borohydride with 1% sodium citrate and 0.05% citric acid was quickly injected into the boiling solution and allowed to boil while stirring under reflux. After 10 min the product was cooled to room temperature.

Fluorescence-enabled electrochemical microscopy. FEEM experiments were carried out on an Olympus IX70 inverted microscope. The excitation source was a Thorlabs M530L2 Collimated LED powered by a DC2100 LED Driver and filtered using a cube with a HQ535/50 excitation filter, a Q565lp dichroic mirror and a HQ610/75 emission filter. An Andor iXon+ EMCCD camera cooled to -80 °C and Andor SOLIS software was used to record and process all videos

and images. The potential across the bipolar electrode array was applied with two Ag/AgCl reference electrodes controlled by a Chem-Clamp potentiostat (Dagan). All reported potentials are referenced vs. Ag/AgCl (3 M KCl).

Preparation and characterization of carbon-fiber microelectrodes (CFEs). Single CFEs can be fabricated following the method published by Strein and Ewing.[66] A 10 μm diameter carbon fiber was aspirated into a piece of glass capillary and pulled using a micropipette puller (Sutter Instrument Co.). The tip of the pipette/fiber was cut and sealed with epoxy. After drying the epoxy, the electrode was further beveled to expose a flat carbon electrode surface. The back end of the pipette was filled with an aqueous solution containing 3 M KCl and redox species at desired concentration. An Ag/AgCl wire was inserted into the back-filled solution to establish an electrical contact.

Preparation and characterization of carbon-fiber microarrays. The bipolar electrode arrays were prepared as previously described.[48] Briefly, carbon fiber pultrusion rods consisting of thousands of insulated individual 6-μm diameter fibers were further sealed in Epo-Tek 301 epoxy and cross sections were then cut and polished to a thickness of ~0.5 mm.

Preparation and characterization of laser-pulled Pt nanoelectrodes. The procedure to prepare the platinum disk nanoelectrodes is described in detail elsewhere.[55,67,68] To briefly summarize, a 25 μm diameter platinum wire was placed in a fused silica capillary tube (O. D.: 1 mm, I. D.: 0.3 mm, Sutter Instrument Co.) and one end sealed closed using an oxygen/hydrogen flame. The fused silica capillary was then placed in a P-2000 laser pipette puller (Sutter Instrument Co.) and vacuum applied to the unsealed end of the capillary. The laser was used to heat and seal the fused silica around the platinum without pulling the capillary. Then the platinum/fused silica assembly was pulled resulting in two ultrasharp tips with the platinum nanowires sealed inside. The tips were then electrically contacted using tungsten wires and conductive silver paste (DuPont). To expose the electrodes a high speed beveling process was employed utilizing a diamond lapping film attached to a rapidly rotating wheel (7500 rpm). The platinum nanoelectrodes were characterized by SEM and steady-state cyclic voltammetry.

Fast-scan cyclic voltammetry. Steady-state voltammograms were recorded using a computer-controlled Dagan Chem-Clamp voltammeter/amperometer and data were recorded using an in-house virtual instrumentation program written in LabView (National instruments) on a desktop PC equipped with a PCI-6251(National Instruments) data acquisition card. A commercially available Ag/AgCl reference electrode (Bioanalytical Sciences, Inc.) was used as reference electrode for all electrochemical data. FSCV data were obtained using a home-built breakout box (UNC Chemistry Electronics Design Facility) equipped with a low noise current amplifier (Electro Optical Components, Inc. model: LCA-10K-500M) running the FSCV software developed by the Wightman group at the University of North Carolina.[69]

Results and discussion

1. Closed bipolar electrochemistry and fluorescence-enabled electrochemical microscopy (FEEM)

This DTRA grant has enabled the Zhang group to study closed bipolar electrochemistry and develop FEEM as a new electrochemical imaging tool for monitoring dynamic redox events

using massive electrochemical arrays. Bipolar electrochemistry is an unconventional form of electrochemistry in that it couples two separate redox processes on the two ends of a single conductor, such as a piece of metal or carbon microwire placed inside a microchannel.[70] The Crooks group has done pioneering work in the use of bipolar electrochemistry in analytical chemistry enabling electrochemical analysis inside tiny microfluidic channels which are otherwise difficult to access. Inspired by Crooks research, the Zhang group has studied electrochemical coupling at closed bipolar microelectrodes and nanoelectrodes.[49]

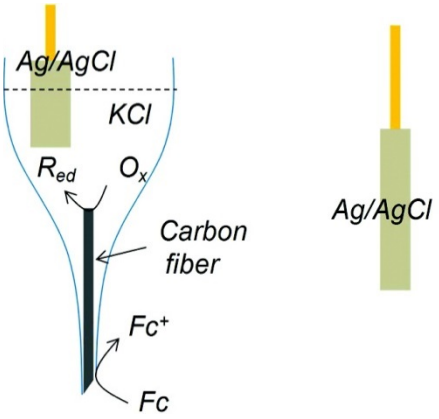

Figure 1: A schematic illustration of an electrolyte-filled CFE used for Fc oxidation.

Although electrolyte-filled carbon-fiber microelectrodes (CFEs) have been widely used as the key microprobe in the field of neurochemistry in the last three decades,[71,72] their working mechanism as to how electrical conductance is established has not been fully understood. The Zhang group has suggested that CFEs are closed bipolar electrodes and their electroanalytical performance in neurochemical sensing is based on cathodic reduction of soluble oxygen species in the electrolyte solution used to fill the inside glass micropipette.[49] Figure 1 illustrates the structure of a KCl-filled CFE. Here the oxidation of ferrocene (Fc) on the electrode surface is coupled to the reduction of oxygen on the inner carbon fiber surface. The kinetic response of CFEs is largely dependent on the coupled cathodic reactions on the inner fiber surface. The Zhang group has discovered that one can fill the CFEs with a redox-containing electrolyte solution, such as 3 M KCl containing 100 mM ferricyanide, in order to promote the kinetic response of electrolyte-filled CFEs.[73]

Based on their work in CFEs, the Zhang group has developed a detailed quantitative understanding of the voltammetric response of a closed bipolar ultramicroelectrode (UME).[50] Their derivation starts from the knowledge that the current magnitudes on the anodic and cathodic poles are the same and the overall voltage bias applied across the closed bipolar electrode is the potential difference on the two poles. The relationship between the applied voltage, E, and the resulting current, i, can be seen from the following equation,

$$E = \left(E_a^{o'} - E_c^{o'}\right) + \frac{RT}{F}\left\{\ln\left(\frac{i}{i_{ss}^a - i}\right) + \ln\left(\frac{-i}{i_{ss}^c + i}\right)\right\} \quad (1)$$

Where $E_a^{o'}$ and $E_c^{o'}$ are formal potentials on the anodic and cathode poles, i_{ss}^a and i_{ss}^c are limiting currents on the two poles, R is the gas constant, T is the absolute temperature, and F is the Faraday's constant. Their theoretical results show that the overall voltammetric current is limited by the pole which has the smaller faradaic current. First, the position of the coupled CV response can be approximated by the difference of the two formal potentials on the two poles. The shape of the voltammetric response, however, depends on both poles. In the simplest case where both redox processes are fast, the overall voltammetric response is dependent on the ratio of the mass-transfer-limited steady-state currents of the two poles. A large limiting current on the excess pole can facilitate the appearance of a fast-looking voltammetric response.

Based on their understanding of closed bipolar electrochemistry, the Zhang group has developed FEEM as a powerful analytical imaging tool using massive electrochemical arrays containing millions of UMEs.[48] FEEM uses a simple concept which is schematically illustrated in Figure 2 (top panel). The key idea is the coupling of two separate faradaic reactions at a closed bipolar electrode, shown with the orange bars in the top panel of Figure 2. A small voltage applied across the insulating membrane drives the coupled reactions allowing electrons to flow from the top to the bottom. The oxidation of an analyte R is coupled to the reduction of an indicator, S, resulting in the generation of a fluorescent molecule, P. In FEEM, fluorescence signal is produced only when an analyte molecule is present and the fluorescence intensity correlates directly to the local concentration of the analyte. In a proof-of-concept experiment, the Zhang group has imaged the formation of a diffusion layer on a gold UME. Figure 2a displays a cross-sectional view of the relative concentration of ferricyanide electrochemically generated on a 12.5 µm diameter UME positioned close to an array of carbon-fiber UMEs. This concentration profile reveals the radial-type diffusion layer generated on the gold UME. The diffusion layer is also simulated and the simulation result (Figure 2b) is in good agreement with that collected with FEEM.

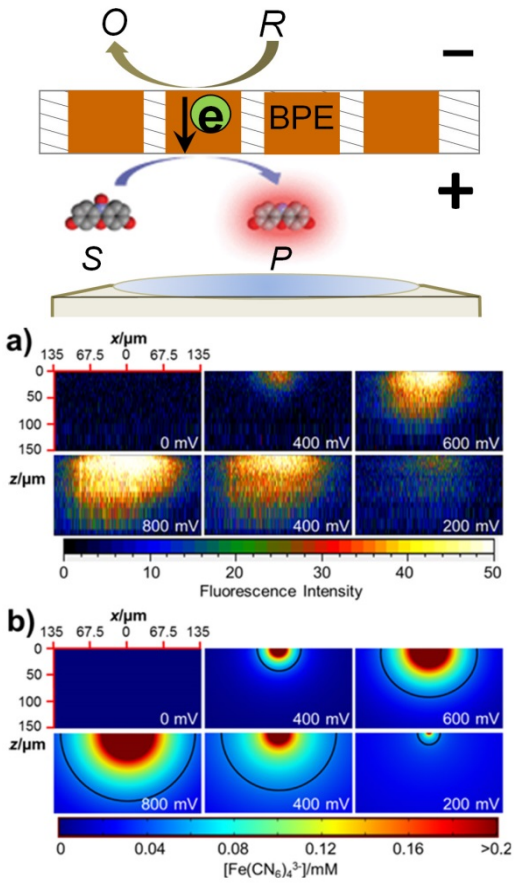

Figure 2. (Upper) a schematic of the bipolar working mechanism of FEEM. (a) A FEEM-generated cross sectional view of the diffusion layer on a 12.5 µm UME in a voltage sweep experiment. (b) The simulated diffusion layer.

The Zhang group has reported the use of FEEM for fast screening of electrocatalysts for the oxidation of hydrogen peroxide (H_2O_2). In a proof-of-concept experiment, the Zhang group used FEEM to image H_2O_2 oxidation on platinum and carbon and the results clearly show that Pt is more active than carbon for this reaction. Figure 3a is a cartoon showing the proposed setup for electrocatalyst screening. Here a carbon UME array was used as the electrode substrate. Part of the array was coated with Pt as an electrocatalytic material which has a higher electrocatalytic activity toward a specific redox reaction. The catalytic activity is reflected by stronger fluorescence intensity at the back of the array where the catalyst is deposited. Figure 3b is an SEM image showing platinum deposited on the carbon array. Figure 3c is the FEEM image showing stronger catalytic activity on the areas where Pt was deposited. Figure 3d shows the result of a control experiment in which an outer sphere redox molecule was used to replace the H_2O_2 species.

The Zhang group has used the concept of closed bipolar electrochemistry and studied the growth of a single metal nanowire inside a short quartz nanochannel.[74] A unique advantage of the bipolar method is the dynamic monitoring and control one can have over the rate of single

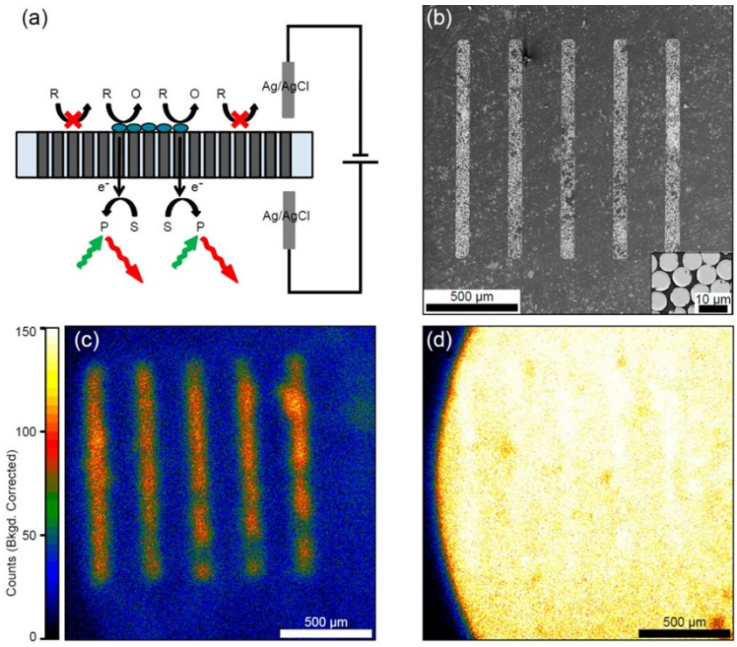

Figure 3. (a) A scheme for FEEM based screening of electrocatalysis. (b) an SEM image of Pt lines deposited on a carbon array. (c) A FEEM image of the same array as in (b) showing higher oxidation current of H2O2 on Pt than on carbon. (d) A FEEM image of the same array showing even oxidation current of FcMeOH.

metal nanowire growth *in situ* without a direct electrical connection. In their work, solutions of a metal precursor and a reducing agent are placed on either side of a silica nanochannel, and a pair of electrodes is used to apply a tunable electric potential across the channel. Metal nanowire growth is initiated by chemical reduction when the two solutions meet and continues until the nanochannel is blocked by the formation of a short metal wire segment. Further nanowire growth is driven by a bipolar electrochemical mechanism which enables the reduction of metal precursor ions at one end of the nanowire and the oxidation of the reducing agent at the other. The growth rate is monitored in real time by simultaneously recording both the faradaic current and optical microscope video and can be adjusted with potential. The final nanowire is solid, electrically insulated, and can be used as a bipolar nanoelectrode.

2. Development and use of nanoelectrodes. The Zhang group has developed metal nanoelectrodes for fundamental electrochemistry as well as nanoparticle collision experiments in collaboration with the Bard group.[75] One of the most popular methods of nanoelectrode fabrication is the laser pulling method in which a piece of metal wire is first sealed inside a glass capillary and then stretched to form an ultrasharp metal electrode. The Zhang group has reported the fabrication and characterization of electrodes down to molecular dimensions (1-3 nm in radii).[55] In this DTRA project, the Zhang group has provided laser-pulled Pt nanoelectrodes for studying single collisional events of gold nanoparticles. The detection of single nanoparticle attachment on a nanoelectrode was observed by the increase in the active electrode area. The attachment of gold nanoparticle-decorated single wall carbon nanotubes (Au-SWCNTs) was studied using ferrocenemethanol oxidation.

The Zhang group has reported the preparation and characterization of ultralong metal nanowires.[76] Single Pt and gold nanowires down to 12 nm in diameter were prepared using a laser pulling method. These laser pulled nanowires have unsurpassed aspect ratios and are highly crystalline with low structural disorder. Additionally, the process used to make these nanowires appears to produce wires that favor low surface energy crystal faces normal to the length of the

wire as exemplified by the {111} crystal face for gold and platinum, which are both FCC crystals. These nanowires can be easily manipulated to make increasingly complex patterns that can be incorporated into functional nano-devices utilizing combinations of the metal nanowires. The nanowires exhibit a very low resistivity approaching that of the bulk metals and also showed fairly high current densities before wire failure.

Using the laser pulling method, the Zhang group has prepared single Pt nanowire electrodes with radii ranging from 25 to 130 nm and studied their electrocatalytic activity toward the oxygen reduction reaction (ORR).[77] Single Pt nanowire electrodes were fabricated by metal deposition and lithography patterning to expose just a small portion (10–20 μm in length) of the nanowire for electrocatalytic studies. These wires were characterized thoroughly using CV, Cu UPD, and SEM. Their results have shown that the ORR activity of Pt nanowires slightly decreases as the nanowire radius is reduced as measured by the onset potential. The ORR current density decreases and the mass activity increases as the wire becomes smaller.

The Zhang group has been recognized by the electrochemical community on their contribution in the area of nanoelectrochemistry. They have been invited by several leading journals in the analytical chemistry field to write review articles.[52,53,54] These include the ACS journal *Analytical Chemistry*, the RSC journal the *Analyst*, and the *Annual Reviews in Analytical Chemistry*.

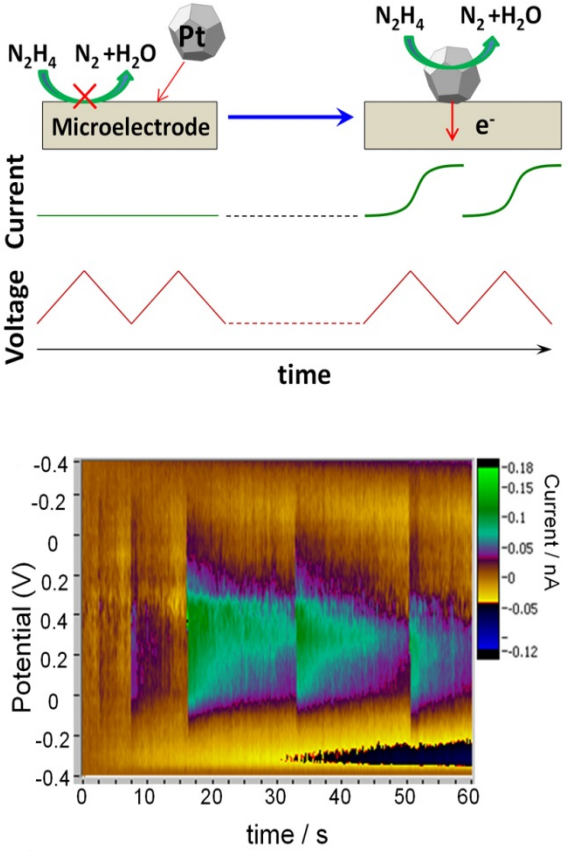

Figure 4. (top) A scheme for FSCV recording of single collision events of Pt nanoparticles on carbon. The oxidation of hydrazine is catalyzed on Pt resulting in an increased CV response on the UME. (bottom) A 60-second FSCV recording showing five collision events recorded on this electrode.

3. Fast-scan cyclic voltammetry for single-nanoparticle collision

The Zhang group has pioneered the use of fast-scan cyclic voltammetry (FSCV) to study single collision events of electrocatalytic nanoparticles.[56] In addition, they have reported the use of FSCV to extract useful electron-transfer kinetics of redox reactions on single nanoparticles.[57] One of the major limitations in conventional nanoparticle collision experiments is the use amperometric recording which uses a constant potential on the recording UME. Although this has an exceedingly high temporal resolution, no chemical information can be obtained. Recognizing this limitation, the Zhang group has recorded single collisional events of 4-nm Pt nanoparticles and 12 nm Au nanoparticles on a carbon UME using FSCV. As shown in the upper panel of Figure 4, this method allows one to scan the potential on the recording carbon UME while recording the faradaic current on the same electrode in nanoparticle collision experiments. The collision and adsorption of an additional single catalytic nanoparticle increases the total faradaic current on the UME. Such events can

be immediately recorded and plotted on the current-voltage-time plot as a sudden color change, as shown in the bottom panel of Figure 4. Here, five 4-nm Pt nanoparticles were recorded during this 60-second recording period. Each collision event can be clearly seen from the color plot. One can easily obtain the entire CV of each nanoparticle from FSCV recording. The subsequent CV analysis can reveal excellent chemical information of the nanoparticles. For example, the Zhang group has shown that they can easily distinguish Au and Pt nanoparticles in a mixed solution.

In a more recent publication, the Zhang group has extended the use of FSCV to analyze electron-transfer kinetics of hydrazine oxidation on single Pt and Au nanoparticles when they collide onto a carbon electrode.[57] The use of FSCV has enabled investigation and better understanding of electrocatalytic activity of single metal nanoparticles of different sizes, shapes and capping ligands for hydrazine oxidation and how the data can be misinterpreted if mass transfer is not taken into account. By combining numerical simulation and the FSCV experiments, they have shown that key kinetic parameters, such as the standard electron-transfer rate constant and the charge transfer coefficient can be determined and used to more correctly assess the catalytic activity. They have shown that the capping agent can play a more substantial role in the activity than the nature of the nanoparticle crystallinity and surface orientation.

4. Developing new electrocatalytic methods for detecting single-nanoparticle collision

The Zhang group has developed a new method to detect single collision events of metal nanoparticles on UMEs.[58] This method uses a simple square-wave potential waveform and is based on rapid reduction of AgCl on metal nanoparticle surfaces when a metal nanoparticle collides on the surface of a carbon UME. In the case of Ag, nanoparticles are first oxidized on carbon in the anodic half-cycle in the presence of Cl^- ions to form discrete AgCl patches. Reduction of AgCl takes place in the subsequent cathodic half-cycle when another Ag nanoparticle collides on the UME in the vicinity of the AgCl patches. Detection of both 80-nm Ag and 4-nm Au nanoparticles has been demonstrated although this method can be extended to nanoparticles of other metals. One of the great advantages of this method is that it eliminates the addition and presence of extra redox molecules, such as hydrazine, in the bulk solution. Therefore, the chemical stability of analyte nanoparticles can be less of an issue. This method enables fast and continuous recording of single collision events of Ag nanoparticles for extended time.

5. Mechanistic studies of nanoparticle collisions

In a recent experiment, the Zhang group has observed the presence of ultrashort current spikes associated with single particle collision events in a hydrazine solution containing Pt nanoparticles at nanomolar concentrations.[63] Using a higher bandwidth and faster recording rates (e.g., 100 kHz), a transient current spike can be seen on top of a collision event. The current quickly decays back to the diffusion limited, steady-state hydrazine oxidation current within ~0.5 ms. A 5-second long current-time trace is givenn in Figure 5 (bottom panel) showing seven discrete nanoparticle detection events. The insert is a zoom-in view of the first event displaying the ultrashort current spike observed at the beginning of the event.

They have attributed the short current spikes to the quick oxidation of hydrogen molecules decomposed from hydrazine on Pt nanocatalysts. In addition, they propose that these H_2 molecules are stored in nanometer-sized gas bubbles attached to the surface of Pt nanoparticles prior to collision, as illustrated in the top panel of Figure 5. H_2 molecules are

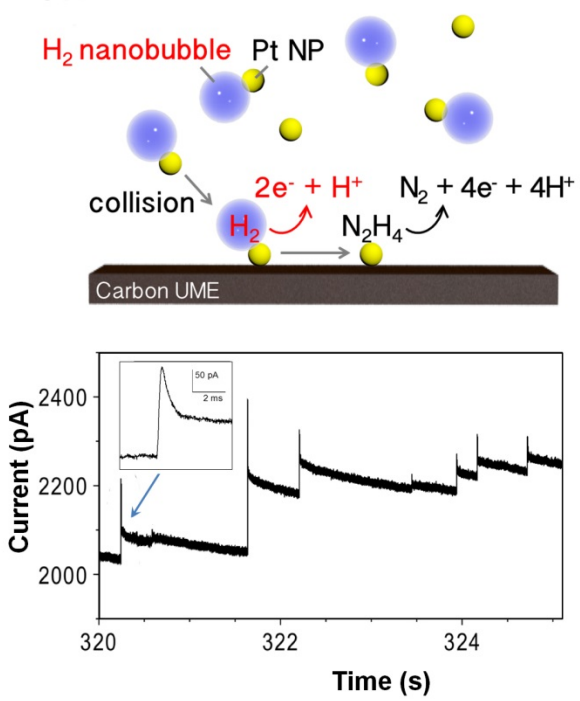

Figure 5. (top) A scheme for the detection of sharp current spikes. H2 nanobubbles are formed due to catalytic decomposition of hydrazine on Pt surfaces. Oxidation and depletion of H_2 is responsible for the sharp current spikes. (bottom) A 5-second recording showing 7 collision events on this electrode.

quickly oxidized and depleted when the nanoparticle/nanobubble ensemble collides with the carbon electrode resulting in a short current spike on top of the long-lasting hydrazine oxidation current.

This work used Pt nanoparticles at up to 2 nM concentration, which is nearly 100 times higher than used in previous studies. The formation of a H_2 nanobubble/Pt nanoparticle ensemble can be understood by the excellent catalytic property of Pt toward hydrazine decomposition which releases H_2 and N_2 and quickly saturate the solution when the solution contains Pt nanoparticles at high concentration. Their proposed mechanism was supported by several experiments. First, in-situ imaging using transmission electron microscopy (TEM) in a liquid cell containing both hydrazine and Pt nanoparticles revealed the presence of individual nanobubbles. Second, these short spikes were detected more frequently in solutions containing higher concentrations of Pt particles, which promoted the formation of H_2 from hydrazine decomposition. Third, short spikes were detected more easily when the hydrazine solution was irradiated with UV and visible lights which also promoted decomposition. Their results show that hydrazine decomposition is a key process in single particle collision experiments especially when excess Pt nanocatalysts are present. Under this condition, generation of gas nanobubbles may play an important role in the detection of single particles. This observation may be more generally extended to the electrocatalytic amplification method because many processes reported so far involved inner sphere redox molecules, such as H_2O_2, H^+, H_2O, BH_4^-, which can produce gaseous molecules as their redox or decomposition products. The formation of nanobubbles from decomposition or faradaic reaction and their possible interactions with the electrode/particle should be carefully considered when studying single particle collisions.

Conclusions

In summary, this DTRA grant has supported the Zhang group to achieve a more comprehensive understanding of single nanoparticle collision electrochemistry through the development and use of several new electroanalytical tools, including structurally well-defined nanoelectrodes, fast-scan cyclic voltammetry, and fluorescence-enabled electrochemical microscopy. The use of molecular-scale laser-pulled Pt and Au nanoelectrodes has enabled study of single nanoparticle collision by area amplification. Furthermore, one can immobilize individual nanoparticles on nanoelectrode surfaces and examine the structure of the same particles following electrochemical measurements. The use of FSCV has offered unique chemical resolution in collision experiments which is otherwise not achievable using amperometry recording. The Zhang group has also

demonstrated the ability to extract useful kinetic information from single-nanoparticle CVs collected during collision experiments.

The development of the fluorescence-enabled electrochemical microscopy in the Zhang group has enabled simultaneous recording from all UMEs in a massive electrochemical array. This can have a significant impact in future experiments in which analyte species are present at very low abundance, e.g., aM. The detection frequency can be greatly increased by monitoring a large number of electrodes, e.g., $>10^6$ using FEEM. In addition to the development of FEEM, the Zhang group has also studied key fundamental aspects of closed bipolar electrochemistry. Recent work in the Zhang group has been focused on mechanistic studies of nanobubbles during nanoparticle collision. Their recent observation of ultrashort current spikes indicates possible presence of hydrogen nanobubbles.

References

[1] Xiao, X.; Bard, A. J. Observing Single Nanoparticle Collisions at an Ultramicroelectrode by Electrocatalytic Amplification. *J. Am. Chem. Soc.* **2007**, *129*, 9610–9612.

[2] Quinn, B. M.; Van 't Hof, P. G.; Lemay, S. G. Time-Resolved Electrochemical Detection of Discrete Adsorption Events. *J. Am. Chem. Soc.* **2004**, *126*, 8360–8361.

[3] Zhou, Y.-G.; Rees, N. V; Compton, R. G. The Electrochemical Detection and Characterization of Silver Nanoparticles in Aqueous Solution. *Angew. Chem. Int. Ed.* **2011**, *50*, 4219–4221.

[4] Robinson, D. A.; Yoo, J. J.; Castañeda, A. D.; Gu, B.; Dasari, R.; Crooks, R. M.; Stevenson, K. J. Increasing the Collision Rate of Particle Impact Electroanalysis with Magnetically Guided Pt-Decorated Iron Oxide Nanoparticles. *ACS Nano* **2015**, *9*, 7583–7595.

[5] Yoo, J. J.; Anderson, M. J.; Alligrant, T. M.; Crooks, R. M. Electrochemical Detection of Insulating Beads at Subattomolar Concentration via Magnetic Enrichment in a Microfluidic Device. *Anal. Chem.* **2014**, *86*, 4302–4307.

[6] Robinson, D. A.; Stevenson, K. J..Uniform Epitaxial Growth of Pt on Fe3O4 Nanoparticles; Synergetic Enhancement to Pt Activity for the Oxygen Reduction Reaction. *J. Mater. Chem. A* **2013**, *1*, 13443.

[7] Kleijn, S. E. F.; Serrano-Bou, B.; Yanson, A. I.; Koper, M. T. M. Influence of Hydrazine-Induced Aggregation on the Electrochemical Detection of Platinum Nanoparticles. *Langmuir* **2013**, *29*, 2054–2064.

[8] Robinson, D. A.; Kondajji, A. M.; Castañeda, A. D.; Dasari, R.; Crooks, R. M.; Stevenson, K. J. Addressing Colloidal Stability for Unambiguous Electroanalysis of Single Nanoparticle Impacts. *J. Phys. Chem. Lett.* **2016**, *7*, 2512–2517.

[9] Alligrant, T. M.; Nettleton, E. G.; Crooks, R. M. Electrochemical Detection of Individual DNA Hybridization Events. *Lab Chip* **2013**, *13*, 349–354.

[10] Alligrant, T. M.; Dasari, R.; Stevenson, K. J.; Crooks, R. M. Electrocatalytic Amplification of Single Nanoparticle Collisions Using DNA-Modified Surfaces. *Langmuir* **2015**, *31*, 11724–11733.

[11] Castaneda, A. D.; Robinson, D. A.; Stevenson, K. J.; Crooks, R. M. Electrocatalytic Amplification of DNA-Modified Nanoparticle Collisions via Enzymatic Digestion. *Chem. Sci.* **2016**, *7*, 6450–6457.

[12] Castañeda, A. D.; Brenes, N.; Kondajji, A. M. Electrochemical Detection of microRNAs via Duplex Specific Nuclease Cleavage of DNA-Modified Pt Nanoparticle Collisions. *In Preparation*.

[13] Bigall, N. C.; Härtling, T.; Klose, M.; Simon, P.; Eng, L. M.; Eychmüller, A. Monodisperse Platinum Nanospheres with Adjustable Diameters from 10 to 100 Nm: Synthesis and Distinct Optical Properties. *Nano Lett.* **2008**, *8*, 4588–4592.

[14] Wang, C.; Daimon, H.; Sun, S. Dumbbell-like Pt–Fe_3O_4 Nanoparticles and Their Enhanced Catalysis for Oxygen Reduction Reaction. *Nano Lett.* **2009**, *9*, 1493–1496.

[15] Xia, Y.; Whitesides, G. M. Soft Lithography. *Annu. Rev. Mater. Sci.* **1998**, *28*, 153–184.

[16] Wehmeyer, K. R.; Wightman, R. M. Cyclic Voltammetry and Anodic Stripping Voltammetry with Mercury Ultramicroelectrodes. *Anal. Chem.* **1985**, *57*, 1989–1993.

[17] Brendel, P. J.; Luther, G. W. I. Development of a Gold Amalgam Voltammetric Microelectrode for the Determination of Dissolved Fe, Mn, O2, and S(-II) in Porewaters of Marine and Freshwater Sediments. *Environ. Sci. Technol.* **1995**, *29*, 751–761.

[18] Zhang, X.; Servos, M. R.; Liu, J. Instantaneous and Quantitative Functionalization of Gold Nanoparticles with Thiolated DNA Using a pH-Assisted and Surfactant-Free Route. *J. Am. Chem. Soc.* **2012**, *134*, 7266–7269.

[19] Zhang, X.; Servos, M. R.; Liu, J. Fast pH-Assisted Functionalization of Silver Nanoparticles with Monothiolated DNA. *Chem. Commun.* **2012**, *48*, 10114–10116.

[20] Robinson, D. A.; Duay, J.; Kondajji, A. M.; Stevenson, K. J. "Mechanistic Aspects of Hydrazine-Induced Pt Colloid Instability and Monitoring Aggregation Kinetics with Nanoparticle Impact Electroanalysis," *Faraday Disc.* **2016**, *193,* 293-312

[21] Kwon, S. J.; Zhou, H.; Fan, F.-R. F.; Vorobyev, V.; Zhang, B.; Bard, A. J. Stochastic Electrochemistry with Electrocatalytic Nanoparticles at Inert Ultramicroelectrodes-Theory and Experiments. *Phys. Chem. Chem. Phys.* **2011,** *13*, 5394-5402.

[22] Quinn, B. M.; van't Hof, P. G.; Lemay, S. G., *J. Am. Chem. Soc.*, **2004**, *126*, 8360.

[23] Xiao, X. Y.; Bard, A. J., *J. Am. Chem. Soc.*, **2007**, *129*, 9610.

[24] Lebegue, E.; Anderson, C. M.; Dick, J. E.; Webb, L. J.; Bard, A. J., *Langmuir*, **2015**, *31*, 11734.

[25] Dunevall, J.; Fathali, H.; Najafinobar, N.; Lovric, J.; Wigstrom, J.; Cans, A. –S.; Ewing, A. G., *J. Am. Chem. Soc.*, **2015**, *137*, 4344.

[26] Cheng, W.; Compton, R. G., *Angew. Chem. Int. Ed.*, **2014**, *53*, 13928.
[27] Kim, B. K.; Boika, A.; Kim, J.; Dick, J. E.; Bard, A. J., *J. Am. Chem. Soc*, **2014**, *136*, 4849.
[28] Dick, J. E.; Hilterbrand, A. T.; Boika, A.; Upton, J. W.; Bard, A. J., *Proc. Natl. Acad. Sci.*, **2015**, *112*, 5303.
[29] Dick, J. E.; Hilterbrand, A. T.; Strawsine, L. M.; Upton, J. W.; Bard, A. J., *Proc. Natl. Acad. Sci.*, **2016**, *113*, 6403.
[30] Sepunaru, L.; Plowman, B. J.; Sokolov, S. V.; Young, N. P.; Compton, R. G., *Chem. Sci*, **2016**, *7*, 3892.
[31] Dick, J. E.; Renault, C.; Bard, A. J., *J. Am. Chem. Soc.*, **2015**, 137, 8376.
[32] Dick, J. E., *Chem. Commun.*, **2016**, *52*, 10906.
[33] Bard, A. J.; Zhou, H.; Kwon, S. J., *Isr. J. Chem.*, **2010**, *50*, 267.
[34] Jung, A. R.; Lee, S.; Joo, J. W.; Shin, C.; Bae, H.; Moon, S. G.; Kwon, S. J. *J. Am. Chem. Soc.*, **2015**, *137*, 1762.
[35] Chen, Q.; Wiedenroth, H. S.; German, S. R.; White, H. W. *J. Am. Chem. Soc.*, **2015**, *137*, 12064.
[36] Boika, A.; Thorgaard, S.N.; Bard, A. J. *J. Phys. Chem. B* **2013**, *117*, 4371-4380.
[37] Park, J. H.; Thorgaard, S. N.; Zhang, B.; Bard, A. J. *J. Am. Chem. Soc.* **2013**, *135*, 5258-5261.
[38] Park, J. H.; Zhou, H.; Percival, S. J.; Zhang, B.; Fan, F.-R. R.; Bard, A. J. *Anal. Chem.* **2013**, *85*, 964-970.
[39] Park, J. H.; Boika, A.; Park H. S.; Lee, H. C.; Bard, A. J. *J. Phys. Chem. C* **2013**, *117*, 6651-6657.
[40] Boika, A.; Bard, A. J. *Anal. Chem.* **2014**, *86*, 11666-11672.
[41] Boika, A.; Bard, A. J. *Anal. Chem.* **2015**, *87*, 4341-4346.
[42] Kim, B.-K.; Boika, A.; Kim, J.; Dick, J. E.; Bard, A. J. *J. Am. Chem. Soc.* **2014**, *136*, 4849-4852.
[43] Dick, J. E.; Lebegue, E.; Strawsine, L. M.; Bard, A. J. *Electroanalysis*, **2016**, *28*, 2320-2326.
[44] Lebegue, E.; Anderson, C. M.; Dick, J. E.; Webb, L. J.; Bard, A. J. *Langmuir,* **2015**, *11734-11739*.
[45] Dick, J. E.; Hilterbrand A. T.; Boika, A.; Upton, J. W.; Bard, A. J. *Proc. Nat. Acad. Sci. U.S.A.* **2015**, *112*, 5303-5308.
[46] Quinn, B. M.; van't Hof, P. G.; and Lemay, S. G. "Time-Resolved Electrochemical Detection of Discrete Adsorption Events" *J. Am. Chem. Soc.* **2004**, *126*, 8360-8361
[47] Xiao, X.; Bard, A. J. "Observing Single Nanoparticle Collisions at an Ultramicroelectrode by Electrocatalytic Amplification" *J. Am. Chem. Soc.* **2007**, *129*, 9610–9612.
[48] Guerrette, J. P.; Percival, S. J.; Zhang, B. "Fluorescence Coupling for Direct Imaging of Electrocatalytic Heterogeneity" *J. Am. Chem. Soc.* **2013***, 135* (2), 855–861 (DOI: 10.1021/ja310401b).
[49] Guerrette, J. P.; Oja, S. M.; Zhang, B. "Coupled Electrochemical Reactions at Bipolar Microelectrodes and Nanoelectrodes" *Anal. Chem.* **2012***, 84*, 1609–1616 (DOI: 10.1021/ac2028672).
[50] Cox, J. T.; Guerrette, J. P.; Zhang, B. "Steady-State Voltammetry of a Microelectrode in a Closed Bipolar Cell" *Anal. Chem.* **2012***, 84* (20), 8797–8804 (DOI: 10.1021/ac302219p).
[51] Xiao, X.; Fan, F.-R. F.; Zhou, J.; Bard, A. J. "Current Transients in Single Nanoparticle Collision Events" *J. Am. Chem. Soc.* **2008**, *130*, 16669–16677.
[52] Oja, S. M.; Fan, Y. S.; Armstrong, C. M.; Defnet, P.; and Zhang, B. "Nanoscale Electrochemistry Revisited" *Anal. Chem.* **2016***, 88*, 414–430 (DOI: 10.1021/acs.analchem.5b04542).
[53] Oja, S. M.; Wood, M.; Zhang, B. "Nanoscale Electrochemistry" *Anal. Chem.* **2013***, 85* (2), 473–486 (DOI: 10.1021/ac3031702).
[54] Fan, Y.; Han, C.; and Zhang, B. "Recent Advances in the Development and Application of Nanoelectrodes" *Analyst,* **2016***, 141*, 5474-5487 (DOI: 10.1039/c6an01285j).
[55] Li, Y.; Bergman, D.; Zhang, B. Preparation and Electrochemical Response of 1-3 nm Pt Disk Electrodes. *Anal. Chem.* **2009**, *81*, 5496–5502.
[56] Guo, Z.; Percival, S. J.; Zhang, B. "Chemically Resolved Transient Collision Events of Single Electrocatalytic Nanoparticles" *J. Am. Chem. Soc.* **2014***, 136*, 8879–8882 (DOI: 10.1021/ja503656a).
[57] Percival, S. J.; and Zhang, B. "Fast-Scan Cyclic Voltammetry Allows Determination of Electron-transfer Kinetic Constants in Single Nanoparticle Collision" *J. Phys. Chem. C* **2016***, 120*, 20536-20546 (DOI: 10.1021/acs.jpcc.5b11330).
[58] Hao, R.; Fan, Y. S.; and Zhang, B. "Electrocatalytic Reduction of Silver Chloride on Single Metal Nanoparticles" *J. Electrochem. Soc.* **2016***, 163*, H3145–H3151 (DOI: 10.1149/2.0191604jes).
[59] Jung, A. R.; Lee, S.; Joo, J. W.; Shin, C.; Bae, H.; Moon, S. G.; Kwon, S. J. "Potential-Controlled Current Responses from Staircase to Blip in Single Pt Nanoparticle Collisions on a Ni Ultramicroelectrode" *J. Am. Chem. Soc.* **2015**, *137*, 1762–1765.
[60] Kang, M.; Perry, D.; Kim, Y. R.; Colburn, A. W.; Lazenby, R. A.; Unwin, P. R. "Time-Resolved Detection and Analysis of Single Nanoparticle Electrocatalytic Impacts" *J. Am. Chem. Soc.* **2015**, *137*, 10902–10905.

[61] Dasari, R.; Robinson, D. A.; Stevenson, K. J. "Ultrasensitive Electroanalytical Tool for Detecting, Sizing, and Evaluating the Catalytic Activity of Platinum Nanoparticles" *J. Am. Chem. Soc.* **2013**, *135*, 570–573.

[62] Singh, S. K.; Xu, Q. "Complete Conversion of Hydrous Hydrazine to Hydrogen at Room Temperature for Chemical Hydrogen Storage" *J. Am. Chem. Soc.* **2009**, *131*, 18032–18033.

[63] Fan, Y. S.; Zhou, M.; Zhang, B. "Ultrashort Current Spikes in Single Nanoparticle Collision" **2017** *in preparation*.

[64] Frens, G. "Controlled Nucleation for the Regulation of the Particle Size in Monodisperse Gold Suspensions" *Nature* **1973**, *241*, 20-22.

[65] Bigall, N. C.; Härtling, T.; Klose, M.; Simon, P.; Eng, L. M.; Eychmüller, A. "Monodisperse Platinum Nanospheres with Adjustable Diameters from 10 to 100 nm: Synthesis and Distinct Optical Properties" *Nano Lett.* **2008**, *8*, 4588-4592.

[66] Strein, T. G.; Ewing, A. G. "Characterization of submicron-sized carbon electrodes insulated with a phenol-allylphenol copolymer" *Anal. Chem.* **1992**, *64*, 1368-1373.

[67] Katemann, B. B.; Schuhmann, W. "Fabrication and Characterization of Needle-Type Pt-Disk Nanoelectrodes." *Electroanalysis* **2002**, *14*, 22–28.

[68] Shao, Y.; Mirkin, M. V.; Fish, G.; Kokotov, S.; Palanker, D.; Lewis, A. "Nanometer-Sized Electrochemical Sensors" *Anal. Chem.* **1997**, *69*, 1627– 1634.

[69] Bucher, E. S.; Brooks, K.; Verber, M.; Keithley, R. B.; Owesson-White, C.; Carroll, S.; Takmakov, P.; McKinney, C. J.; Wightman, R. M. "Flexible Software Platform for Fast-Scan Cyclic Voltammetry Data Acquisition and Analysis" *Anal. Chem.* **2013**, *85*, 10344-10353.

[70] Fosdick S. E.; Knust K. N.; Scida K.; Crooks R. M. "Bipolar Electrochemistry" *Angew. Chem. Int. Ed.* **2013**, *52*, 10438-10456 (DOI: 10.1002/anie.201300947).

[71] Wightman, R.; Jankowski, J.; Kennedy, R.; Kawaoge, K.; Schroeder, T.; Leszczyszyn, D.; Near, J.; Diliberto, E.; Viveros, O. "Temporally resolved catecholamine spikes correspond to single vesicle release from individual chromaffin cells" *Proc. Natl. Acad. Sci. U.S.A.* **1991**, 88, 10754–10758.

[72] Chen, T. K.; Luo, G. O.; Ewing, A. G. "Amperometric Monitoring of Stimulated Catecholamine Release from Rat Pheochromocytoma (PC12) Cells at the Zeptomole Level" *Anal. Chem.* **1994**, *66*, 3031–3035.

[73] Cox, J. T.; Gunderson, C. G.; Zhang, B. "Redox-filled Carbon-Fiber Microelectrodes for Single-Cell Exocytosis" *Electroanalysis* **2013**, 25, 2151-2158.

[74] Wood, M.; Zhang, B. "A Bipolar Electrochemical Method for Dynamic in Situ Control of Single Metal Nanowire Growth" *ACS Nano* **2015***, 9,* 2454–2464 (DOI: 10.1021/acsnano.5b00139).

[75] Park, J. H.; Thorgaard, S. N.; Zhang, B.; Bard, A. J. "Single Particle Detection by Area Amplification – Single Wall Carbon Nanotube Attachment to a Nanoelectrode" *J. Am. Chem. Soc. CommEd,* **2013***, 135* (14), 5258–5261 (DOI: 10.1021/ja4000917).

[76] Percival, S. J.; Vartanian, N.; Zhang, B. "Laser-pulled Ultralong Platinum and Gold Nanowires" *RSC Adv.* **2014***, 4*, 10491–10498 (DOI: 10.1039/c3ra47207h).

[77] Percival, S. J.; Zhang, B. "Electrocatalytic Reduction of Oxygen at Single Platinum Nanowires" *J. Phys. Chem. C* **2013***, 117* (27), 13928–13935 (DOI: 10.1021/jp400407n).